eng

MDPI

Article

Penta-Hybrid Nanofluid Transport and Irreversibility in Stenotic Arteries Under Caputo–Fabrizio Fractional Dynamics

Basim M. Makhdoum

Mechanical Engineering Department, College of Engineering and Architecture, Umm Al-Qura University, P.O. Box 5555, Makkah 21955, Saudi Arabia; bmmakhdoum@uqu.edu.sa; Tel.: +966-509555535

Abstract

The current research first investigates the flow in the fractional order of a vertical artery with atherosclerosis using a Casson-based penta-hybrid nanofluid. Gold (Au), copper (Cu), silver (Ag), magnesium oxide (MgO), and alumina (Al_2O_3) nanoparticles are dispersed in blood to make the hybrid nanofluid. It is assumed that the flow is very pulsatile. The mathematical model is constructed by using differential forms of the conservation laws of mass, momentum, energy, and irreversibility analysis. By applying the mild stenosis approximation, the governing equations are transformed into dimensionless form. To generalize the classical model to its fractional counterpart, the Caputo–Fabrizio fractional derivative (C-FFD) is employed. Closed-form solutions for the velocity and temperature fields are realized by the joint application of the Laplace and Hankel transforms. The impact of essential physical parameters on velocity, temperature, and entropy generation is displayed through figures. The physical significance of enhanced thermal characteristics is shown, emphasizing their potential relevance to thermal regulation, targeted drug delivery, and minimization of irreversible energy losses in biomedical flow systems. The velocity profile elevates with the increase in the Casson parameter, while the temperature drops as the fractional-order parameter rises. Entropy generation is observed to amplify with the increasing values of the thermodynamic parameter in question, whereas an opposite tendency is seen for the Bejan number. The Bejan number decreases as the control parameter becomes higher. The novelty of the present investigation lies in the simultaneous incorporation of Caputo–Fabrizio fractional dynamics, penta-hybrid nanoparticle suspension, and entropy generation analysis in a stenosed arterial configuration. Unlike existing fractional Casson blood flow models that primarily focus on single or hybrid nanofluids, the present framework highlights the synergistic enhancement of thermal transport and irreversibility control achieved through penta-hybrid nanoparticles, which may be relevant for advanced biomedical and targeted therapeutic applications.

Keywords: penta-hybrid nanofluid; Casson fluid; Caputo–Fabrizio fractional derivative; entropy generation; Bejan number

Check for updates

Academic Editor: Rajinder Pal

Received: 12 January 2026
Revised: 27 January 2026
Accepted: 6 February 2026
Published: 10 February 2026

Copyright: © 2026 by the author. Licensee MDPI, Basel, Switzerland. This article is an open access article distributed under the terms and conditions of the Creative Commons Attribution (CC BY) license.

1. Introduction

The introduction has been revised to clarify that penta-hybrid nanofluids allow synergistic enhancement of thermal conductivity, rheological control, and entropy minimization beyond what is achievable with tri- or tetra-hybrid systems. Hybrid nanofluids are a newly promising class of engineered fluids aimed at improving heat transport beyond what is possible with regular nanofluids. Mono-nanofluids and bi-hybrid nanofluids use one or two types of nanoparticles, respectively, but multi-hybrid nanofluids with three or

more nanoparticles have been recently developed. Among them, penta-hybrid nanofluids composed of five different nanoparticle materials are an innovative and highly efficient category because of their synergistic thermal, chemical, and rheological properties.

The use of five nanoparticles such as metals (Au, Cu, Ag), metal oxides (MgO, Al_2O_3), or other functional nano-additives allows for the simultaneous improvement of thermal conductivity, heat capacity, stability, optical activity, and magnetic or catalytic response. Every nanoparticle has its own role: metallic nanoparticles give the best thermal conductivity; metal oxides increase stability and heat capacity; and noble metals improve electrical and thermal performance. So, in a combined state, these nanoparticles create a fluid with very good heat transfer capabilities, enhanced energy transport, and higher thermophysical performance than conventional nanofluids. Penta-hybrid nanofluids are receiving more and more attention in the fields of biomedical engineering, thermal energy systems, cooling technologies, and physiological flow applications.

Fractional calculus, sophisticated constitutive models, and hybrid numerical–analytical methods have become effective means for reflecting memory effects, nonlocal behavior, and time-dependent responses in such fluids. Hence, understanding the dynamics of penta-hybrid nanofluids is crucial for the construction of dependable models that accurately mirror real physiological and engineering systems. Choi, et al. [1] presented nanofluids, which are recognized as the first generation of advanced HTF. Ahmad et al. [2] and Mohyud-Din et al. [3] brought about the second generation, which is referred to as hybrid nanofluids, and the third generation consists of modified or further enhanced nanofluids, as per the report of Abbasi et al. [4]. These three generations of nanofluids are being used in various fields of modern technology. They are utilized in electronics, biomedical engineering, and drug preservation systems to ensure stability and prevent degradation during storage. Furthermore, these materials can be found in the fields of aerodynamics, chemo- and cancer-diagnosis studies, as well as in paints, appliances, and other industrial processes that involve hybrid or modified nanoparticle mixtures.

Due to their multi-purpose and outstanding heat-transfer features, discovering the behavior of nanofluids has become imperative for numerous industrial and engineering applications. Such increasing importance has been a source of encouragement for researchers and experts in fluid dynamics to focus deeply on this topic. To be more specific, the number of studies [5–9] that have been conducted on blood-based nanofluids with modified nanoparticles to emphasize their potential in biomedical applications is quite large.

The term biomagnetic fluid dynamics (BFD) refers to an emerging area of fluid mechanics that studies the reaction of biological fluids to magnetic fields, with a special focus on blood [10]. This domain of research is of great significance to medical science and has the potential to be used in such areas as delivering drugs through the use of magnetized particles, controlling severe bleeding, and helping in the treatment of cancerous tumors [11,12]. One of the main reasons for cancer cells being attacked by the biomagnetic response of blood is the magnetic properties of hemoglobin molecules, according to Shahzad et al. [13].

Experimentally, Shabbir et al. [14] examined the forced flow of Bingham plastic nanofluids through a stenosed artery under the effect of periodic body acceleration along with an external magnetic field. Majee and Shit [15] went on to deepen the understanding of blood flow in the case of arterial stenosis, whereas Akbar and Butt [16] carried out the numerical analyses of non-steady blood flow and the related heat transfer mechanisms.

Generally, blood can be treated as a Newtonian fluid when it is moving in huge arteries at high shear rates, as it is a homogeneous fluid whose viscosity does not vary [17,18]. On the other hand, Liepsch [19] argued that blood might show non-Newtonian features even in large vessels if the shear rate is sufficiently low. Blood in such instances—especially if the flow is slow—may be successfully simulated as a Casson fluid [20]. Therefore, some

works [21–23] have resorted to the Casson fluid model to comprehend blood circulation in stenosed arteries, which are particularly low shear rate regimes. By using Laplace and Hankel transform methods, Ali et al. [24] have constructed a fractional-order model describing a Casson fluid. Application of these mathematical means enabled them to garner exact solutions that exhibit the memory effects and the hereditary nature of fractional-order processes; thus, the model becomes more relevant to biological fluid flows. Moreover, He et al. [25] have used computational fluid dynamics (CFD) to vividly represent the blood flow in arteries under different physiological conditions. The analysis of the heat and mass transfer phenomena that resulted from this process is of primary importance in the modeling of physiological and industrial processes.

Electro-magnetohydrodynamics (EMHD) deals with peculiar aspects of fluid dynamics where an externally imposed magnetic field and an electric field govern fluid motion. Theoretical, computational, and experimental works have paid much attention to the impact of magnetic (MHD) or electric (EHD) fields on normal fluid and blood flow. These alterations come about because the momentum equations reveal extra force terms, such as the Lorentz and Coulomb forces, which are the forces acting on the fluid.

Magnetohydrodynamics (MHD) has been employed in various biomedicine methods such as tumor remedy, bleeding arrest, magnetic drug targeting, hyperthermia for cell killing, and magnetic endoscopy [26]. Akbar and Butt [27] analyzed the influence of magnetic fields on copper nanoparticles in a stenosed (narrowed) arterial segment with wall slip effects. Mekheimer et al. [28] studied how the concentration of copper nanoparticles affects blood flow in an artery with overlapping stenoses when an external magnetic field is applied. Their results indicated that the wall shear stress increases with a larger Ha number and decreases with a smaller Gr number. Electrohydrodynamics (EHD) has shown vast potential in medical diagnostics, particle separation, cell-based therapies, drug delivery, and biochemical processes [29]. Electrokinetic carriage arises since the vessel wall becomes electrically charged, as blood, an electrically conducting fluid, flows through it. According to the principle of electroneutrality, the blood within the electric double layer (EDL) near the wall carries a charge conflicting with that of the wall. One of the earliest theoretical investigations of electrokinetic flow was carried out by Burgreen and Nakache [30], who studied flow in very small rectangular microvessels. More recently, Saravani and Kalteh [31] used a lattice Poisson–Boltzmann model to examine the behavior of a Newtonian nanofluid.

Entropy can be generated through various mechanisms, including mechanical friction, Joule heating, thermal resistance, viscous interactions between fluids, and mass dispersion. According to the second law of thermodynamics, in a reversible method, the net change in the system's entropy is zero. The first law of thermodynamics, on the other hand, asserts that energy is always conserved. Still, the second law revolves around the idea that energy tends to spread out on its own, and energy gradients—differences of temperature, pressure, or concentration—are getting smaller all the time. That means if you look at a system, the net energy will be the same; however, its performance power will be less because part of the energy will be more evenly distributed. This increase in disorder or randomness is what the second law of the system entropy refers to. Further understanding of entropy generation can be found in references [32–35].

To simulate phenomena existing in nature, fractional differential equations are the most common choice, since such equations provide an option for a system to be remembered or inherited with the effects of its past, as in dynamic systems. The idea of fractional calculus was proposed for the first time by L'Hôpital in 1695. Unlike classical calculus, which includes integer-order differentiation, fractional calculus involves derivatives of arbitrary (non-integer) order. Nowadays fractional differential equations are frequently referred to because they have immense potential in physics and engineering and may

become the solution to many problems in these scientifically based areas. The usage of fractional calculus is not restricted to the modeling of memory effects in systems; it is also a suitable tool for such processes as electrochemical, electromagnetic, and heat diffusion and conduction [36].

Our investigation delves into the fractional-order time derivative model of blood flow through arteries under the influence of a magnetic field and coupled heat transfer based on the non-Newtonian Casson fluid model. The fractional derivatives are used to represent the axial velocity and temperature relations and, following that, they are resolved by numerical and analytical methods. It is noted that blood flow in arteries carrying mono-, hybrid-, and ternary nanoparticles has been studied extensively through fractional models; however, no significant research has been done on the extension of fractional operators to higher-order nanoparticles, such as tetra- and penta-component mixtures. Normally, in real-life biomedical and engineering situations, scientists use mono-nanofluids or simple hybrid nanofluids to enhance heat transfer and flow performance. Yet, these fluids are still burdened with serious limitations such as low thermal conductivity, poor stability, limited tunability, and insufficient control in complicated physiological environments like blood flow through stenosed arteries. The problems become quite serious in human-related systems where, for instance, efficient temperature regulation, less flow resistance, and controlled thermodynamic irreversibility are of vital importance, such as in hyperthermia treatment, targeted drug delivery, blood heating/cooling, and magnetic biomedical procedures.

Penta-hybrid nanofluids facilitate the increase of heat transfer capacity, effective viscosity management, and entropy reduction at the same time, by virtue of synergistic interaction between multiple nanoparticles. As compared to tri- or tetra-hybrid systems, penta-hybrid mixtures provide a greater range of thermophysical property tuning possibilities. This advantage can be very helpful in the biomedical field where such properties need to be optimized together with heat transfer and flow control. In order to break the barriers, this research communicates the idea of a penta-hybrid nanofluid, which contains five different nanoparticles (Au, Cu, Ag, MgO, Al_2O_3), rather than a single or a dual nanoparticle that is normally found in the instances of the previous studies. The multi-component nanofluid reveals such synergistic thermal and rheological characteristics, which so far could not be attained by conventional nanofluids. The use of metal and metal-oxide nanoparticles together results in drastic increase of thermal conductivity, better heat diffusion, higher stability, and stronger electromagnetic response.

Additionally, when compared to current models that depend on classical integer-order derivatives, our research features the Caputo–Fabrizio fractional operator, thus allowing a more accurate depiction of blood's memory-dependent behavior. This emphasizes the physiological accuracy of the proposed model. Furthermore, the article fills the gap in the factional-order blood flow research by coupling it with entropy generation and the Bejan number, a sophisticated combination that has never before been considered for penta-hybrid nanofluids.

Here we are moving forward with the use of fractional derivatives to model blood flow phenomena by involving complex nanoparticle systems. Our work is primarily targeted at achieving analytical solutions to the momentum and energy equations created by the Laplace and Hankel transforms, and at the same time their reverses, using the positive roots of Bessel functions to enable numerical calculations. Tables 1 and 2 contain the thermophysical characteristics of the penta nanoparticles and their base fluids that are used as the basis for the study.

Table 1. Configurations of penta hybrid-nanofluid.

Structures	Penta Hybrid-Nanofluid
Dynamic viscosity	$\mu_{pthnf} = \frac{\mu_f}{(1-\phi_1)^{2.5}(1-\phi_2)^{2.5}(1-\phi_3)^{2.5}(1-\phi_4)^{2.5}(1-\phi_5)^{2.5}}$ $\dagger_4 = \frac{\mu_{thnf}}{\mu_f}$.
Density	$\rho_{pthnf} = (1-\phi_5)\rho_{tehnf} + \rho_{s5}\phi_5$ $\rho_{tehnf} = (1-\phi_4)\rho_{thnf} + \rho_{s4}\phi_4$ $\rho_{thnf} = (1-\phi_3)\rho_{hnf} + \rho_{s3}\phi_3$ where $\rho_{hnf} = (1-\phi_2)\rho_{nf} + \rho_{s2}\phi_2$ and $\rho_{nf} = (1-\phi_1)\rho_f + \rho_{s1}\phi_1$ $\dagger_3 = \frac{\rho_{pthnf}}{\rho_f}$.
Thermal conductivity	$\kappa_{pthn\,f} = \kappa_{tehnf}\left(\frac{\kappa_{s5}+(m-1)\kappa_f+(m-1)(\kappa_{s5}-\kappa_f)\phi_5}{\kappa_{s5}+(m-1)\kappa_f-(\kappa_{s5}-\kappa_f)\phi_5}\right)$ $\kappa_{tehn\,f} = \kappa_{thnf}\left(\frac{\kappa_{s4}+(m-1)\kappa_f+(m-1)(\kappa_{s4}-\kappa_f)\phi_4}{\kappa_{s4}+(m-1)\kappa_f-(\kappa_{s4}-\kappa_f)\phi_4}\right)$ $\kappa_{thn\,f} = \kappa_{hnf}\left(\frac{\kappa_{s3}+(m-1)\kappa_f+(m-1)(\kappa_{s3}-\kappa_f)\phi_3}{\kappa_{s3}+(m-1)\kappa_f-(\kappa_{s3}-\kappa_f)\phi_3}\right)$ where $\kappa_{hn\,f} = \kappa_{nf}\left(\frac{\kappa_{s2}+(m-1)\kappa_f+(m-1)(\kappa_{s2}-\kappa_f)\phi_2}{\kappa_{s2}+(m-1)\kappa_f-(\kappa_{s2}-\kappa_f)\phi_2}\right)$ and $\kappa_{n\,f} = \left(\frac{\kappa_s+\kappa_f(m-1)+(m-1)(\kappa_s-\kappa_f)\phi_1}{\kappa_s+(m-1)\kappa_f-(\kappa_s-\kappa_f)\phi}\right)\kappa_f$. $\dagger_2 = \frac{\kappa_{pthnf}}{\kappa_f}$.
Heat capacity	$(\rho C_p)_{pthnf} = (1-\phi_5)(\rho C_p)_{tehnf} + \phi_5(\rho C_p)_{s5}$ $(\rho C_p)_{tehnf} = (1-\phi_4)(\rho C_p)_{thnf} + \phi_4(\rho C_p)_{s4}$ $(\rho C_p)_{thnf} = (1-\phi_3)(\rho C_p)_{hnf} + \phi_3(\rho C_p)_{s3}$ where $(\rho C_p)_{hnf} = (1-\phi_2)(\rho C_p)_{nf} + \phi_2(\rho C_p)_{s2}$ and $(\rho C_p)_{nf} = (1-\phi_1)(\rho C_p)_f + \phi_1(\rho C_p)_{s1}$. $\dagger_1 = \frac{(\rho C_p)_{pthnf}}{(\rho C_p)_f}$.
Electrical conductivity	$\sigma_{pthnf} = \sigma_{tehnf}\left(\frac{\sigma_{s5}(1+2\phi_5)+2\sigma_f(1-\phi_5)}{\sigma_{s5}(1-\phi_5)+\sigma_f(2+\phi_5)}\right)$ $= \sigma_{thnf}\left(\frac{\sigma_{s4}(1+2\phi_4)+2\sigma_f(1-\phi_4)}{\sigma_{s4}(1-\phi_4)+\sigma_f(2+\phi_4)}\right)$ $\sigma_{thnf} = \sigma_{hnf}\left(\frac{\sigma_{s3}(1+2\phi_3)+2\sigma_f(1-\phi_3)}{\sigma_{s3}(1-\phi_3)+\sigma_f(2+\phi_3)}\right)$ where $\sigma_{hnf} = \sigma_{nf}\left(\frac{\sigma_{s2}(1+2\phi_2)+2\sigma_f(1-\phi_2)}{\sigma_{s2}(1-\phi_2)+\sigma_f(2+\phi_2)}\right)$ and $\sigma_{nf} = \sigma_f\left(\frac{\sigma_{s1}(1+2\phi_1)+2\sigma_f(1-\phi_1)}{\sigma_{s1}(1-\phi_1)+\sigma_f(2+\phi_1)}\right)$. $\dagger_6 = \frac{\sigma_{pthnf}}{\sigma_f}$.
Thermal expansion coefficient	$(\rho\alpha_T)_{pthnf} = (1-\phi_5)(\rho\alpha_T)_{tehnf} + \phi_5(\rho\alpha_T)_{s5}$ $(\rho\alpha_T)_{tehnf} = (1-\phi_4)(\rho\alpha_T)_{thnf} + \phi_4(\rho\alpha_T)_{s4}$ $(\rho\alpha_T)_{thnf} = (1-\phi_3)(\rho\alpha_T)_{hnf} + \phi_3(\rho\alpha_T)_{s3}$ where, $(\rho\alpha_T)_{hnf} = (1-\phi_2)(\rho\alpha_T)_{nf} + \phi_2(\rho\alpha_T)_{s2}$ and $(\rho\alpha_T)_{nf} = (1-\phi_1)(\rho\alpha_T)_f + \phi_1(\rho\alpha_T)_{s1}$ $\dagger_5 = \frac{(\rho\alpha_T)_{pthnf}}{(\rho\alpha_T)_{nf}}$.

Table 2. Penta hybrid nanoparticles and base fluid.

Characteristics	Blood	Gold	Copper	Alumina	Silver	Magnesium Oxides
$\rho\ (kg/m^3)$	1063	19320	8933	3971	10500	3580
$\kappa\ \left(\frac{W}{mK}\right)$	0.493	315	402	40.01	429	30
$\alpha_T \times 10^{-6}\left(\frac{1}{K}\right)$	1.81	14	1.67	8.61	18	10
$C_p\left(\frac{J}{(kg\ K)^1}\right)$	3595	129	386	766	235	879
$\sigma\ \left(\frac{1}{(S \cdot m)}\right)$	6.671×10^{-1}	4.11×10^{7}	5.96×10^{7}	35×10^{6}	6.3×10^{7}	5.392×10^{-7}

With the help of these analytical solutions, we are able to produce numerical results for velocity and temperature under different physical conditions, which also help us understand the effects of nanoparticles on flow and heat transfer by graphical representation. There have been various studies that have separately looked into fractional-order blood flow models, hybrid nanofluids, and entropy generation. However, there still has not been much research on their combined effect in a stenosed arterial environment. The joint effects of penta-hybrid nanoparticles, Caputo–Fabrizio fractional derivatives with non-singular kernel, and irreversibility measures such as entropy generation and Bejan number have not been simultaneously studied in the literature. The present work, which integrates all these aspects, hence represents a novel line of research and offers a comprehensive tool for investigating complex bio-thermal transport phenomena.

Importantly, to the best of our knowledge, no prior studies have investigated fractional-order blood flow models in coincidence with entropy generation and the Bejan number, making this research a novel contribution to the field.

The main objectives of the present study are outlined as follows:

- A fluid containing five different nanoparticles transfers heat more effectively than one with only a single type. This motivates its use in the study.
- The main focus is to boost how well the fluid can conduct and manage heat.
- Although gold nanoparticles have strong physical properties, their actual biomedical applications in blood flow are not widely discussed, leaving a research gap.
- The Caputo–Fabrizio fractional derivative is cast off to capture fluid behavior more accurately than traditional (integer-order) derivatives.

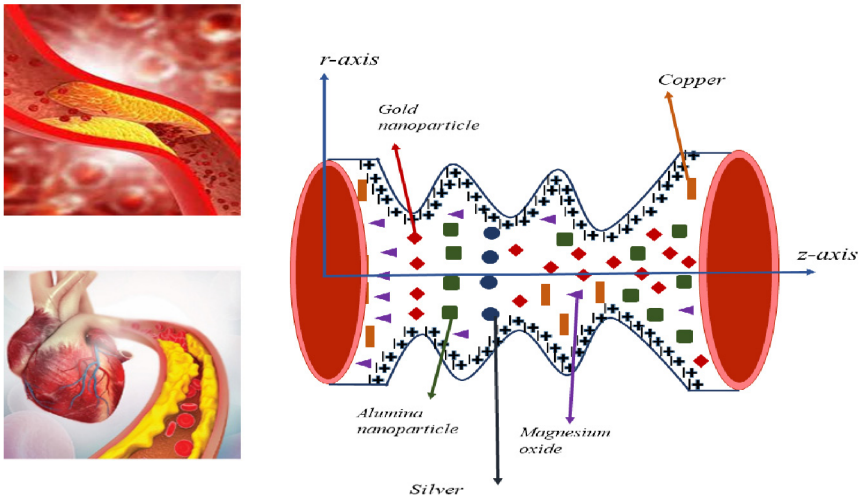
2. Physical Structure and Problem Formulation

2.1. Flow Geometry

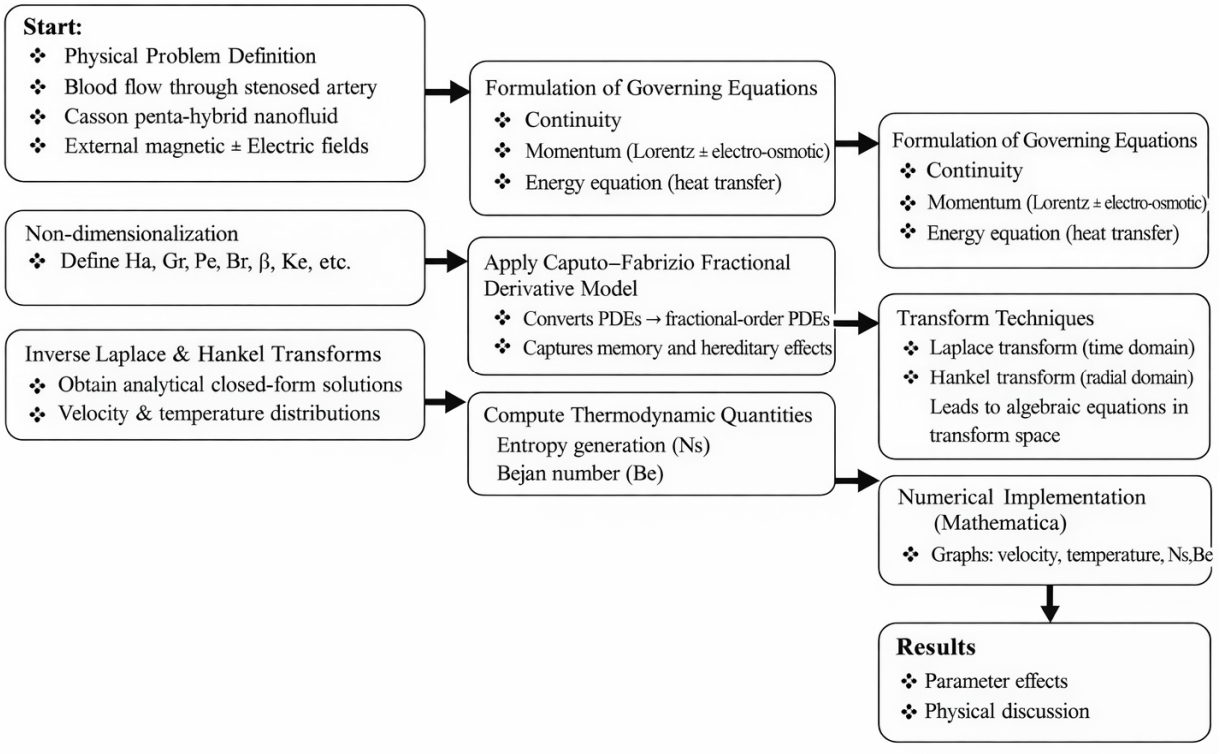
A schematic depiction of a stenosed artery containing multiple stenoses is illustrated in Figure 1a. The central objective of this study is to examine the behavior of penta-hybrid nanofluids enriched with penta-nanoparticles as they flow through a stenotic artery of length L under the influence of an externally applied MF. To carry out this investigation, the following assumptions are adopted: the blood is modeled as a two-dimensional, incompressible Casson fluid, and the stenosed arterial segment is considered axisymmetric. Based on these assumptions, the corresponding geometric profile of the artery is formulated. The stenosis that is considered here can be regarded as the initial development of atherosclerosis, which leads to a very slight narrowing of arteries. It is basically the first stage to atherosclerosis in medium-sized arteries. This kind of geometry

is used in many hemodynamic studies in theory in order to obtain the main features of the flow while keeping the geometry simple.

$$\widetilde{R}\left(\widetilde{z}\right) = \begin{cases} \left(\widetilde{R}_0 - \hat{\chi}\widetilde{z}\right)\left[1 - \frac{\widetilde{\delta}_s}{2\widetilde{R}_0}\left(1 + cos\frac{2\pi}{\widetilde{L}_0}\left(\widetilde{z} - \widetilde{d} - \frac{\widetilde{L}_0}{2}\right)\right)\right], \widetilde{d} \le \widetilde{z} \le \widetilde{d} + 4\widetilde{L}_0 \\ \left(\widetilde{R}_0 - \hat{\chi}\widetilde{z}\right), \quad \text{otherwise} \end{cases} \quad (1)$$



(**a**)



(**b**)

Figure 1. (**a**) Schematic of blood flow. (**b**) Flow chart.

The mild stenosis approximation can only be used for small-to-moderate arterial constrictions, usually up to 20–30% reduction in arterial radius, when higher-order nonlinear geometric effects can be neglected.

2.2. Basic Flow Equation

We analyze an unsteady, incompressible, and axially symmetric blood flow model within an artery affected by stenosis. In this investigation, five different types of nanoparticles (Au, Cu, Ag, MgO, and Al_2O_3) are dispersed in the blood (the base fluid), forming a penta-nanofluid mixture. This advanced nanofluid is considered in order to enhance the thermal and flow characteristics of blood. According to Newton's second law, the governing momentum equations incorporate the influence of electromagnetic forces, while Maxwell's equations and the dynamics of alluring atoms determine the strength and distribution of the applied MF (see [23]).

This study investigates blood flow through an inclined artery containing a localized stenosis. The flow is modeled as unsteady, axisymmetric, and incompressible, consistent with the physiological characteristics of blood under in vivo conditions. To enhance the thermofluidic performance of the system, five distinct nanoparticles are dispersed within the base fluid, forming a penta-nanofluid that is expected to improve heat transfer, support flow regulation, and offer potential advantages for drug-delivery applications. The governing formulation is derived from Newton's second law to capture the force–motion balance of the fluid, while the externally applied magnetic field is incorporated through Maxwell-based electromagnetic relations to characterize the interaction between the magnetic field and the magnetic-responsive constituents of the suspension.

$$\rho_{pthnf}\frac{\partial \widetilde{u}}{\partial \widetilde{t}} = -\frac{\partial \widetilde{p}}{\partial \widetilde{z}} + \mu_{pthnf}\left(1+\frac{1}{\beta}\right)\left[\frac{\partial^2 \widetilde{u}}{\partial \widetilde{r}^2} + \frac{1}{\widetilde{r}}\frac{\partial \widetilde{u}}{\partial \widetilde{r}}\right] + \rho_{pthnf}X\left(\widetilde{t}\right) - \sigma_{pthnf}B_0^2\widetilde{u} + \rho_e E_z + (\rho\alpha_T)_{pthnf} g sin\beta\, 1\left(\widetilde{T}-T_\infty\right), \quad (2)$$

$$\left(\rho\widetilde{C}_p\right)_{pthnf}\left[\frac{\partial \widetilde{T}}{\partial \widetilde{t}} + \widetilde{u}\frac{\partial \widetilde{T}}{\partial \widetilde{z}} + v\frac{\partial \widetilde{T}}{\partial \widetilde{r}}\right] = \kappa_{pthnf}\left[\frac{\partial^2 \widetilde{T}}{\partial \widetilde{r}^2} + \frac{1}{\widetilde{r}}\frac{\partial \widetilde{T}}{\partial \widetilde{r}} + \frac{\partial^2 \widetilde{T}}{\partial \widetilde{z}^2}\right] + \widetilde{Q}_s. \quad (3)$$

Viscous resistance in the momentum equation refers to the impact of blood rheology; the magnetic term thus resulting from Lorentz force represents damping; buoyancy is considered due to the thermal gradient in a blood vessel; and finally, the electro-osmotic term models the effect of the externally applied electric field on the charged fluid layers. The expression describing the acceleration of a body subjected to a vibrating situation can be written as follows:

$$X\left(\widetilde{t}\right) = \widetilde{A}_0 cos\left(\widetilde{k}\widetilde{t} + \Phi_0\right). \quad (4)$$

The boundary conditions of the proposed model are based on the following assumptions:

$$\begin{aligned} &\widetilde{u}(\widetilde{r},\widetilde{t}) = 0, \quad \widetilde{T}(\widetilde{r},\widetilde{t}) = T_w \quad \text{when} \quad \widetilde{r} = R(\widetilde{z}) \\ &\frac{\partial \widetilde{u}}{\partial \widetilde{r}} = \frac{\partial \widetilde{T}}{\partial \widetilde{r}} = 0 \qquad\qquad\qquad \text{at} \quad \widetilde{r} = 0 \end{aligned} \quad (5)$$

2.3. External Applied Electric Field

Electro-osmotic phenomena have the greatest impact in microvascular and bio-microfluidic systems; however, by including them here, a comprehensive mathematical model is being presented which is able to capture the effect of electrically induced flow modulations that can be either naturally occurring or externally controlled in biomedical and therapeutic settings. When an external electric field (EF) is pragmatic along the axis of the nanofluid flow, an electric double layer (EDL) forms near the vessel walls, producing a net electrical body force. As a result, the electrolyte develops an equilibrium charge density.

$$\widetilde{\rho}_e = \widetilde{z}_0\widetilde{e}_0\left(\widetilde{n}_+ = \widetilde{n}_-\right) \quad (6)$$

The concentrations of cations and anions, assuming that the electric double layer (EDL) does not overlap, are governed by the Boltzmann distribution and are expressed as $\widetilde{n}_+$ and $\widetilde{n}_-$.

$$\widetilde{n}_\pm = \widetilde{n}_0 exp\left(\mp\frac{\widetilde{z}_0\widetilde{e}_0\widetilde{\psi}}{\widetilde{T}_0\widetilde{k}_b}\right) \tag{7}$$

$$\nabla^2\widetilde{\psi} = \frac{1}{\widetilde{r}}\frac{\partial\widetilde{\psi}}{\partial\widetilde{r}} + \frac{\partial^2\widetilde{\psi}}{\partial\widetilde{r}^2} = -\frac{\widetilde{\rho}_e}{\varepsilon} \tag{8}$$

where ε is dielectric constant.

$$\nabla^2\widetilde{\psi} = \frac{1}{\widetilde{r}}\frac{\partial\widetilde{\psi}}{\partial\widetilde{r}} + \frac{\partial^2\widetilde{\psi}}{\partial\widetilde{r}^2} = \frac{2\widetilde{z}_0\widetilde{e}_0\widetilde{n}_0}{\varepsilon} sinh\left(\mp\frac{\widetilde{z}_0\widetilde{e}_0\widetilde{\psi}}{\widetilde{T}_0\widetilde{k}_b}\right) \tag{9}$$

The description of Debye length is

$$\widetilde{\lambda}_D = \sqrt{\frac{\varepsilon\widetilde{T}_0\widetilde{k}_b}{2\widetilde{z}_0^2\widetilde{e}_0^2\widetilde{n}_0}} \tag{10}$$

Electrical potential energy represented by $\left(\left|\widetilde{z}_0\widetilde{e}_0\widetilde{\psi}\right| \le \left|\widetilde{T}_0\widetilde{k}_b\right|\right)$. Then, the Debye–Hückel approximation (DHA) $sinh\left(\frac{\widetilde{z}_0\widetilde{e}_0\widetilde{\psi}}{\widetilde{T}_0\widetilde{k}_b}\right) \approx \frac{\widetilde{z}_0\widetilde{e}_0\widetilde{\psi}}{\widetilde{T}_0\widetilde{k}_b}$ is applied. Thus

$$\frac{1}{\widetilde{r}}\frac{\partial\widetilde{\psi}}{\partial\widetilde{r}} + \frac{\partial^2\widetilde{\psi}}{\partial\widetilde{r}^2} = \widetilde{\kappa}^2\widetilde{\psi} \tag{11}$$

The BCs become:

$$\widetilde{\psi} = \widetilde{\psi}_w \quad \text{at} \quad \widetilde{r} = R(z), \qquad \frac{\partial\widetilde{\psi}}{\partial\widetilde{r}} = 0 \quad \text{at} \quad \widetilde{r} = 0 \tag{12}$$

$\widetilde{\psi}_w$ characterizes the Zeta function. Subsequently, we use the non-dimensional parameters $\psi = \frac{\widetilde{\psi}}{\widetilde{\psi}_w}$ and $r = \frac{\widetilde{r}}{\widetilde{R}_0}$; the non-dimensional version of the equation is

$$\frac{1}{r}\frac{\partial\psi}{\partial r} + \frac{\partial^2\psi}{\partial r^2} = \kappa^2\psi \tag{13}$$

$$\frac{\partial\psi}{\partial r} = 0 \text{ when } r = 0 \qquad \psi = \psi_w \text{ when } r = R(z). \tag{14}$$

Ke characterizes the thickness of the electric double layer. For the prescribed boundary conditions given in Equation (25), the electric potential distribution can be obtained analytically by applying the corresponding governing equation.

$$\psi(r) = \frac{l_0(Ker)}{l_0(KeR)} \tag{15}$$

In addition, $Ke = \frac{\widetilde{R}_0}{\widetilde{\lambda}_D}$ is the Debye length representing the thickness of the electric double layer in an electrolyte. When the artery radius is large compared to the Debye length, electrokinetic forces become more pronounced. Conversely, if the Debye length

is relatively large, these effects weaken. This ratio therefore determines the strength of electrokinetic interactions in blood–electrolyte systems.

The momentum and temperature equations are transformed into their non-dimensional forms by using the following dimensionless variables.

$$r=\frac{\widetilde{r}}{R_0},z=\frac{\widetilde{z}}{R_0},\omega=\frac{\omega_2}{\omega_1},t=\frac{u_0\widetilde{t}}{R_0},u=\frac{\widetilde{u}}{u_0},p=\frac{\widetilde{p}}{\rho u_0^2},\Theta=\frac{\widetilde{T}-T_\infty}{T_w-T_\infty},Q_0=\frac{R_0\widetilde{Q}_0}{u_0\rho\widetilde{C}p(T_w-T_\infty)},\wp_0=\frac{R_0\widetilde{A}_0}{u_0^2},k=\frac{\widetilde{k}R_0}{u_0},u_e=\frac{\widetilde{E}_{\widetilde{z}}\widetilde{\varepsilon}\widetilde{\psi}_w}{\widetilde{\mu}_f}. \tag{16}$$

Equation (16) introduces a non-dimensional variable used to simplify the governing equations. When this variable is inserted into Equations (2) and (3), the equations are rewritten in a dimensionless form. After this substitution, the tilde symbols (which usually indicate dimensionless quantities) are removed to make the expressions cleaner. At this stage, appropriate assumed forms (trial functions or similarity transformations) are introduced to further reduce or transform the equations.

$$\dagger_3\alpha^*\frac{\partial u}{\partial t}=-\frac{\partial p}{\partial z}+\dagger_4\left(1+\frac{1}{\beta}\right)\left[\frac{\partial^2u}{\partial r^2}+\frac{1}{r}\frac{\partial u}{\partial r}\right]+\dagger_3\,\dagger_0\,cos(kt+\Phi_0)-\dagger_6Ha^2u+Ke^2\psi(r)+\dagger_5Grsin\beta 1\Theta, \tag{17}$$

$$\dagger_1P\,e\frac{\partial\Theta}{\partial t}=\dagger_2\left[\frac{\partial^2\Theta}{\partial r^2}+\frac{1}{r}\frac{\partial\Theta}{\partial r}\right]+Q_s, \tag{18}$$

The Hartmann number represents the Ha = $\frac{\sigma_fB_0^2R_0^2}{\mu_f}$, the Eckert number signifies the $\frac{u_0^2}{(C_p)_f(T_w-T_\infty)^2}$ and the Grashof number symbolizes the $\frac{\rho_f(\alpha_T)_fg(T_w-T_\infty)R_0^2}{\mu_fu_0}$.

The BCs in the dimensionless form are

$$u(r,t)=0,T(r,t)=T_w\ \text{ at }\ r=R(z),\quad \frac{\partial u}{\partial r}=\frac{\partial T}{\partial r}=0\ \text{ at }\ r=0. \tag{19}$$

The pumping action of the heart drives blood through the cardiovascular system, creating a pressure gradient throughout the vessels. In this model, the pressure gradient consists of two components: a constant (steady) part and a time-dependent (pulsatile) part, expressed as follows:

$$-\frac{\partial\breve{p}}{\partial\widetilde{z}}=\breve{a}_0+\breve{a}_1cos\left(\widetilde{\omega}\widetilde{t}\right), \tag{20}$$

The main equations of momentum and temperature expressed within the framework of the time-fractional model are given as follows:

$$\dagger_3\,\alpha^*D_t^\varsigma u=-\frac{\partial p}{\partial z}+\dagger_4\left(1+\frac{1}{\beta}\right)\left[\frac{\partial^2u}{\partial r^2}+\frac{1}{r}\frac{\partial u}{\partial r}\right]+\dagger_3\,\wp_0cos(kt+\Phi_0)-\dagger_6\,Ha^2u+Ke^2\frac{l_0(Ker)}{l_0(KeR)}+\dagger_5\,Grsin\beta\,1\Theta, \tag{21}$$

$$\dagger_1\,PeD_t^\varsigma\Theta=\ \dagger_2\left[\frac{\partial^2\Theta}{\partial r^2}+\frac{1}{r}\frac{\partial\Theta}{\partial r}\right]+Q_s. \tag{22}$$

In the case when the Caputo description is stated as

$$D_t^\alpha f(r,t)=\frac{1}{1-\alpha}\int_0^\tau exp\left(\frac{-\alpha(\tau-t)}{1-\alpha}\right)f'(\tau)dt, \tag{23}$$

The Caputo–Fabrizio fractional derivative is used here mainly due to its non-singular exponential kernel feature, which prevents the occurrence of power-law singularities and thus, at the same time, it can be considered a more realistic representation of the memory effects occurring in biological transport processes, with $\varsigma(0<\varsigma<1)$. In reality,

the fractional-order parameter provides a deeper understanding of flow behavior. The fractional-order model offers a more detailed representation compared to the traditional integer-order model.

3. The Solution to the Problem

The Laplace transform proves to be highly effective for solving the time-fractional models under consideration. The series solutions represent the velocity and temperature distributions within a blood vessel stenosis, subjected to fractional memory and various external forces. Moreover, this solution scheme allows a privileged interpretation of changes in the parameters through physiological terms. As reported, series solutions exhibit rapid convergence, which means that only a few terms are needed for achieving high numerical accuracy. The convergence of the series was ascertained by raising the truncation levels until insignificant differences were found in the resultant profiles.

$$\begin{aligned} \dagger_3\, \alpha^* S^{\varsigma} u(r,s) = {} & \dagger_4 \left(1+\tfrac{1}{\beta}\right)\left[\tfrac{\partial^2 u(r,s)}{\partial r^2}+\tfrac{1}{r}\tfrac{\partial u(r,s)}{\partial r}\right] \\ & + \wp_0\, \dagger_3 \left[\tfrac{scos\phi_0 - ksin\phi_0}{k^2+s^2}\right] + \tfrac{b_0}{s} + \tfrac{b_1 s}{s^2+w^2} \\ & - \dagger_6\, Ha^2 u(r,s) + \tfrac{Ke^2 \psi(r)}{s} + \dagger_5\, Gr\, sin\beta \Theta(r,s), \end{aligned} \tag{24}$$

$$\dagger_1\, P\, e\, S^{\varsigma}\Theta(r,s) = \dagger_2 \left[\frac{\partial^2 \Theta(r,s)}{\partial r^2} + \frac{1}{r}\frac{\partial \Theta(r,s)}{\partial r}\right] + Q_s. \tag{25}$$

Applying the BCs, Equations (26) and (27) can be expressed as follows.

$$\begin{aligned} & \left[S^{\varsigma} + \tfrac{\dagger_4}{\dagger_3\, \alpha^*}\left(1+\tfrac{1}{\beta}\right) r_n^2 + \tfrac{\dagger_6}{\dagger_3\, \alpha^*} Ha^2\right] u_H(r_n,s) \\ = {} & \tfrac{\wp_0}{\alpha^*}\left[\left(\tfrac{scos\phi_0 - ksin\phi_0}{k^2+s^2}\right) + \tfrac{b_0}{\dagger_3\, \alpha^* s} + \tfrac{b_1 s}{\dagger_3\, \alpha^*(s^2+\omega^2)}\right]\tfrac{J_1(r_n)}{r_n} + \tfrac{r_n K e^2}{s\left(r_n^2+K^2\right)\dagger_3 \alpha^*} J_1(r_n) + \tfrac{\dagger_5}{\dagger_3 \alpha^*} Gr sin\beta\, 1\Theta_H(r,s), \end{aligned} \tag{26}$$

$$\dagger_1\, P\, e\, S^{\varsigma}\Theta_H(r_n,s) = \dagger_2\left(-r_n^2 \Theta_H(r_n,s)\right) + \frac{Q_s}{s}\frac{J_1(r_n)}{r_n}. \tag{27}$$

where $u_H(r_n,s) = \int_0^1 r u(r,s) J_0(r r_n) dr$ signifies finite Hankel transform $u_H(r_n,s)$ and $r_n, (n = 1,2,3,4,5,....)$

$$\Theta_H(r_n,s) = \frac{Q_s}{P\, e\, s\left[\frac{\dagger_2 r_n^2}{\dagger_1 Pe} + S^{\varsigma}\right]}\frac{J_1(r_n)}{r_n}. \tag{28}$$

From Equation (16), we obtain

$$\begin{aligned} u_H(r_n,s) = {} & \left[\tfrac{b_0}{s} + \tfrac{b_1 s}{s^2+\omega^2} + \wp_0\, \dagger_3 \left(\tfrac{scos\phi_0 - ksin\phi_0}{k^2+s^2}\right)\right]\tfrac{1}{\dagger_3\, \alpha^*(S^{\alpha}+B_{2n})}\tfrac{J_1(r_n)}{r_n} + \\ & \left[\tfrac{\dagger_5 Q_s Grsin\beta 1}{\dagger_3 \alpha^* P\, e\, s(S^{\varsigma}+B_{1n})(S^{\varsigma}+B_{2n})}\right]\tfrac{J_1(r_n)}{r_n} + \tfrac{r_n K e^2}{s\left(r_n^2+K^2\right)\dagger_3 \alpha^*} J_1(r_n), \end{aligned} \tag{29}$$

and rearranging Equation (29) as

$$\begin{aligned} u_H(r_n,s) = {} & \left[\tfrac{b_0}{\dagger_3\, \alpha^*}\left(\tfrac{s^{-1}}{S^{\varsigma}+B_{2n}}\right) + \tfrac{b_1}{\dagger_3\, \alpha^*}\left(\tfrac{s}{s^2+\omega^2}\right)\left(\tfrac{1}{S^{\varsigma}+B_{2n}}\right)\right]\tfrac{J_1(r_n)}{r_n} \\ & + \tfrac{\wp_0}{\alpha^*}\left(cos\phi_0\left(\tfrac{s}{k^2+s^2}\right)\left(\tfrac{1}{S^{\varsigma}+B_{2n}}\right) - sin\phi_0\left(\tfrac{k}{k^2+s^2}\right)\left(\tfrac{1}{S^{\varsigma}+B_{2n}}\right)\right)\tfrac{J_1(r_n)}{r_n} \\ & + \tfrac{\dagger_5 Gr Q_s sin\beta}{\dagger_3 \alpha^* Pe(B_{1n}-B_{2n})}\left[\tfrac{s^{-1}}{S^{\varsigma}+B_{2n}} - \tfrac{s^{-1}}{S^{\varsigma}+B_{1n}}\right]\tfrac{J_1(r_n)}{r_n} + \tfrac{s}{S^{\varsigma}+B_{2n}}\tfrac{r_n K e^2}{\left(r_n^2+K^2\right)\dagger_3 \alpha^*} J_1(r_n). \end{aligned} \tag{30}$$

Similarly ordering Equation (28), it becomes

$$\Theta_H(r_n,s) = \frac{\dagger_2\, Q_s}{\dagger_1}\left[\frac{s^{-1}}{S^{\varsigma}+B_{1n}}\right]\frac{J_1(r_n)}{P\, e\, r_n}. \tag{31}$$

where $B_{1n} = \frac{\dagger_2 r_n^2}{\dagger_1 Pe}$, $B_{2n} = \left[\frac{\dagger_4}{\dagger_3 \alpha^*}\left(1+\frac{1}{\beta}\right) r_n^2 + \frac{\dagger_6}{\dagger_3 \alpha^*} Ha^2\right]$.

Exploiting the ILT on Equation (20), it becomes

$$u_H(r_n,t) = [\lambda_{1n}(t) + \lambda_{2n}(t) - \lambda_{3n}(t) + \lambda_{4n}(t) + \lambda_{5n}(t)]\frac{J_1(r_n)}{r_n} + +\lambda_{5n}(t)J_1(r_n), \quad (32)$$

where

$$\left.\begin{array}{l} \lambda_{1n}(t) = \frac{b_0}{\dagger_3\ \alpha^*} R_{\varsigma-1}(-B_{2n},t), \\ \lambda_{2n}(t) = \left(\frac{b_1}{\dagger_3\ \alpha^*} cos(\omega t)\ F_\varsigma(-B_{2n},t) + \frac{\wp_0 cos\phi_0}{\alpha^*} cos(kt)\ F_\dagger(-B_{2n},t)\right), \\ \lambda_{1n}(t) = \frac{b_0}{\dagger_3\ \alpha^*} R_{\varsigma-1}(-B_{2n},t), \\ \lambda_{3n}(t) = \left(\frac{\wp_0}{\alpha^*} sin\phi_0\right) sin(kt)\ F_\varsigma(-B_{2n},t), \\ \lambda_{4n}(t) = \frac{\dagger_5\ GrQ_s sin\beta\ 1}{\dagger_3\ \alpha^* Pe(B_{1n}-B_{2n})}[R_{\alpha-1}(-B_{2n},t) - R_{\alpha-1}(-B_{1n},t)], \\ \lambda_{5n}(t) = \frac{r_n K e^2}{\left(r_n^2+K^2\right)\dagger_3 \alpha^*}[R_\varsigma(-B_{2n},t)]. \end{array}\right\} \quad (33)$$

Based on Equation (31)

$$\Theta_H(r_n,t) = F_{5n}(t)\frac{J_1(r_n)}{r_n}, \quad (34)$$

$$F_{5n}(t) = \frac{\dagger_2\ Q_s}{\dagger_1\ P\ e} R_{\varsigma-1}(-B_{1n},t), \quad (35)$$

The Laplace transform of a special fractional derivative can be represented using the formulations of Riemann–Liouville and Hartley, or alternatively, Lorenzo and Hartley.

$$F_\varsigma(-z,t) = L^{-1}\left(\frac{1}{S^\varsigma + z}\right) = \sum_{n=0}^{\infty} \frac{(-z)^n t^{(n+1)\varsigma-1}}{\Gamma(n+1)\varsigma - 1}, \varsigma > 0, \quad (36)$$

$$R_{\varsigma,v}(-z,t) = L^{-1}\left(\frac{s^{-1}}{S^\varsigma + z}\right) = \sum_{n=0}^{\infty} \frac{(-z)^n t^{(n+1)\varsigma-1-v}}{\Gamma(n+1)\varsigma - 1 - v}, Re(\varsigma - v) > 0, \quad (37)$$

The Rabotnov–Hartley and Lorenzo–Hartley functions are generalized fractional integral/relaxation functions commonly used in fractional calculus to model memory and hereditary effects in complex fluids.

In this step, Equations (26) and (27) are still expressed in the Hankel transform space. By applying the inverse Hankel transform, we convert the solutions back into the physical (spatial) domain, allowing us to obtain the final analytical forms of velocity, temperature, or concentration as required.

$$u(r,t) = 2\sum_{n=1}^{\infty} \frac{J_0(rr_n)}{J_1^2(r_n)}[\lambda_{1n}(t) + \lambda_{2n}(t) - \lambda_{3n}(t) + \lambda_{4n}(t) + \lambda_{5n}(t)]. \quad (38)$$

$$\Theta(r,t) = 2\sum_{n=1}^{\infty} \frac{J_0(rr_n)}{J_1^2(r_n)} F_{5n}(t). \quad (39)$$

The Casson fluid model describes a type of non-Newtonian fluid with a yield stress, commonly used to model blood flow. By assigning the corresponding parameter value in the general hybrid or non-Newtonian fluid model, the equations simplify, reflecting the rheological behavior of a Casson fluid. This simplification allows the governing equations to directly represent Casson fluid flow characteristics, making analytical or numerical analysis more straightforward.

$$F_1(-z,t) = e^{-zt}, R_{1,v}(-z,t) = z^{-1}\left(1 - e^{-zt}\right), \quad (40)$$

The velocity and temperature distributions can be expressed in analytical form as follows.

$$u(r,t) = 2(\sum_{n=1}^{\infty} \frac{J_0(rr_n)}{J_1^2(r_n)}[\hbar_{1n}(t) + \hbar_{2n}(t) - \hbar_{3n}(t) + \hbar_{4n}(t) + \hbar_{5n}(t)]), \tag{41}$$

$$\Theta(r,t) = 2\sum_{n=1}^{\infty} \frac{J_0(rr_n)}{J_1^2(r_n)} G_{5n}(t), \tag{42}$$

The skin friction represented as

$$C_f = \frac{\tau_w}{\rho_f \widetilde{u}_0^2}; \text{ where } \tau_w = -\mu_{pthnf}\left(1 + \frac{1}{\beta}\right)\left[\frac{\partial \widetilde{u}}{\partial \widetilde{r}}\right]_{r=R_0}. \tag{43}$$

The Nusselt number becomes

$$Nu = \frac{R_0 q_w}{\kappa_f(T_w - T_\infty)}; \text{ where } q_w = -\kappa_{pthnf}\left[\frac{\partial \widetilde{T}}{\partial \widetilde{r}}\right]_{r=R_0}. \tag{44}$$

$$C_f = -\frac{\mu_{pthnf}}{\mu_f}\left(1 + \frac{1}{\beta}\right)\left[\frac{\partial u}{\partial r}\right]_{r=1}; \tag{45}$$

$$Nu = -\frac{\kappa_{pthnf}}{\kappa_f}\left[\frac{\partial \Theta}{\partial r}\right]_{r=1}; \tag{46}$$

4. Entropy Generation

Entropy production in human blood flow can be viewed as a measure of the inefficiency arising from viscous heat generation, uneven temperature distribution, and the presence of an electromagnetic field. Thus, to ensure proper thermal regulation and low mechanical stress in arteries, the production of entropy must be kept at a minimum. Mathematically, entropy generation is expressed as:

$$E_{gen} = \frac{\kappa_{pthnf}}{\Im}\left(\frac{\partial \widetilde{T}}{\partial \widetilde{r}}\right)^2 + \frac{\tau_{rz}}{T_m}\left(\frac{\partial \widetilde{u}}{\partial \widetilde{r}}\right) + \frac{\sigma_{pthnf}}{\Im} B_0 \widetilde{u}^2, \tag{47}$$

The non-dimensional form of entropy generation is expressed as follows:

$$\tau_{rz} = \mu_{pthnf}\left(1 + \frac{1}{\beta}\right)\left(\frac{\partial \widetilde{u}}{\partial r}\right), \zeta = \frac{T_w - T_\infty}{\Im}. \tag{48}$$

$N_G = \frac{E_{gen}}{S_G}$, where $S_G = \frac{\kappa_f(T_w - T_\infty)^2}{\Im^2 R_0^2}$ utilizing S_G in N_G, we acquired

$$N_G = \frac{\Im^2 R_0^2}{\kappa_f(T_w - T_\infty)^2}(E_{gen}), \tag{49}$$

$$E_{gen} = \dagger_2\left(\frac{\partial \Theta}{\partial r}\right)^2 + \frac{\dagger_4\, Br}{\zeta}\left(1 + \frac{1}{\beta}\right)\left(\frac{\partial u}{\partial r}\right)^2 + \dagger_6\, BrHa^2u^2. \tag{50}$$

A key thermodynamic measure used to evaluate the relative importance of these effects is the Bejan number (*Be*). The Bejan number can also be expressed in an alternative mathematical form, which highlights the balance between heat-transfer irreversibility and fluid-friction irreversibility. The Bejan number variations in the current study agree with the previous ones in biofluid dynamics; however, the addition of penta-hybrid

nanoparticles causes a greater deviation, as their presence significantly improves the heat transfer mechanism.

$$Be = \frac{\dagger_2 \left(\frac{\partial \Theta}{\partial r}\right)^2}{\dagger_2 \left(\frac{\partial \Theta}{\partial r}\right)^2 + \frac{\dagger_4 \, Br}{\zeta}\left(1 + \frac{1}{\beta}\right)\left(\frac{\partial u}{\partial r}\right)^2 + \dagger_6 \, Ha^2 Bru^2} \tag{51}$$

Furthermore, the stepwise flow chart is given in Figure 1b, for the current technique.

5. Results and Analysis

Numerical results for velocity, temperature, entropy generation, and the Bejan number were obtained using Mathematica and are presented graphically in Figures 2–14. These results illustrate how key physical parameters influence blood flow, heat transfer, and thermodynamic irreversibility. The effects of parameters such as the Hartmann number, fractional parameter, and Casson fluid parameter were systematically analyzed, with specific values for the gold, copper, aluminum oxide, magnesium oxide and silver nanoparticles used in the computations.

The velocity distributions are illustrated in Figures 2–7. Figure 2 indicates that when the fractional parameter increases, the velocity of the fluid rises accordingly. This occurs because fractional derivatives incorporate memory effects, meaning the present motion of blood depends partly on its past state. A higher fractional order reduces resistance within the fluid, resulting in enhanced velocity. This trend is observed for both pure blood and penta-hybrid nanofluid, with the nanofluid exhibiting an even greater rise due to improved thermal and rheological characteristics. Figure 3 further reveals that suspending nanoparticles in blood (forming a penta-hybrid nanofluid) significantly increases the velocity. Nanoparticles enhance thermal conductivity and energy transport within the fluid, reducing viscous forces and allowing the blood to flow more easily. In Figure 4, the Casson fluid parameter demonstrates a notable influence: increasing this parameter effectively reduces the yield stress of the fluid. As a result, the apparent viscosity decreases, which allows the blood to flow faster. This is a common behavior in shear-thinning non-Newtonian fluids like blood. Figure 5 shows a rise in velocity with increasing Grashof number. Physically, this means that stronger thermal buoyancy forces are generated when temperature differences increase. These buoyancy forces push the fluid upward, helping it overcome viscous resistance and thereby accelerating the flow. Figure 6 illustrates that intensified electric double-layer (EDL) effects lead to increased axial velocity. The EDL introduces electro-osmotic forces that assist the fluid motion, enhancing the overall flow rate. Figure 7 demonstrates that higher Hartmann numbers reduce the velocity. A larger Hartmann number corresponds to a stronger magnetic field, which generates a Lorentz force acting opposite to the direction of flow. This magnetic drag slows the fluid. Clinically, this principle is important: magnetic fields can be used to regulate or suppress blood flow in medical treatments, such as managing atherosclerotic conditions or targeting heated tissues. Figure 8 shows that increasing the Peclet number results in a reduction in temperature. A higher Peclet number implies stronger convective heat transport, meaning heat is carried away more efficiently by the moving fluid. As a result, the temperature of the system decreases. In Figure 9, an increase in the fractional parameter leads to a decrease in temperature. This reflects the effect of memory-based heat transfer: the fluid's thermal response becomes more sensitive to past states, which moderates temperature rise and enhances heat dissipation. Figure 10 illustrates that higher metabolic heat generation increases the temperature. Physiologically, this corresponds to the body producing additional heat during metabolic activity to maintain thermal balance and support biochemical processes.

The variations of entropy generation and Bejan number corresponding to different physical parameters are illustrated in Figures 11–14. Figure 11 reveals that a rise in the Brinkman number (Br) significantly enhances the entropy generation rate. This is because a larger Brinkman number represents stronger viscous dissipation, which converts more mechanical energy into thermal energy. However, the Bejan number decreases under this condition, as the contribution from fluid friction becomes dominant compared to heat-transfer irreversibility. Figure 12 also shows that increasing the Casson fluid parameter (β) reduces entropy generation. A larger Casson parameter weakens the non-Newtonian resistance, resulting in lower viscous dissipation and hence reduced thermal losses. Consequently, the Bejan number increases because the irreversibility shifts from fluid friction-dominated to heat transfer-dominated processes. Figure 13a,b illustrates that increasing the temperature difference parameter decreases entropy generation but increases the Bejan number. A higher temperature ratio effectively reduces the temperature gradient in the system, lowering heat-transfer irreversibility. With lower entropy generation, the Bejan number increases, indicating that heat-transfer irreversibility becomes more significant relative to frictional effects. Figure 14 shows that applying a magnetic field (higher Hartmann number) increases entropy generation at the core of the artery while having minimal effect near the walls. The Lorentz force opposes fluid motion and introduces additional ohmic heating, which increases total irreversibility. The Bejan number exhibits the opposite trend. Its reduction implies that magnetic and viscous effects dominate over heat-transfer irreversibility.

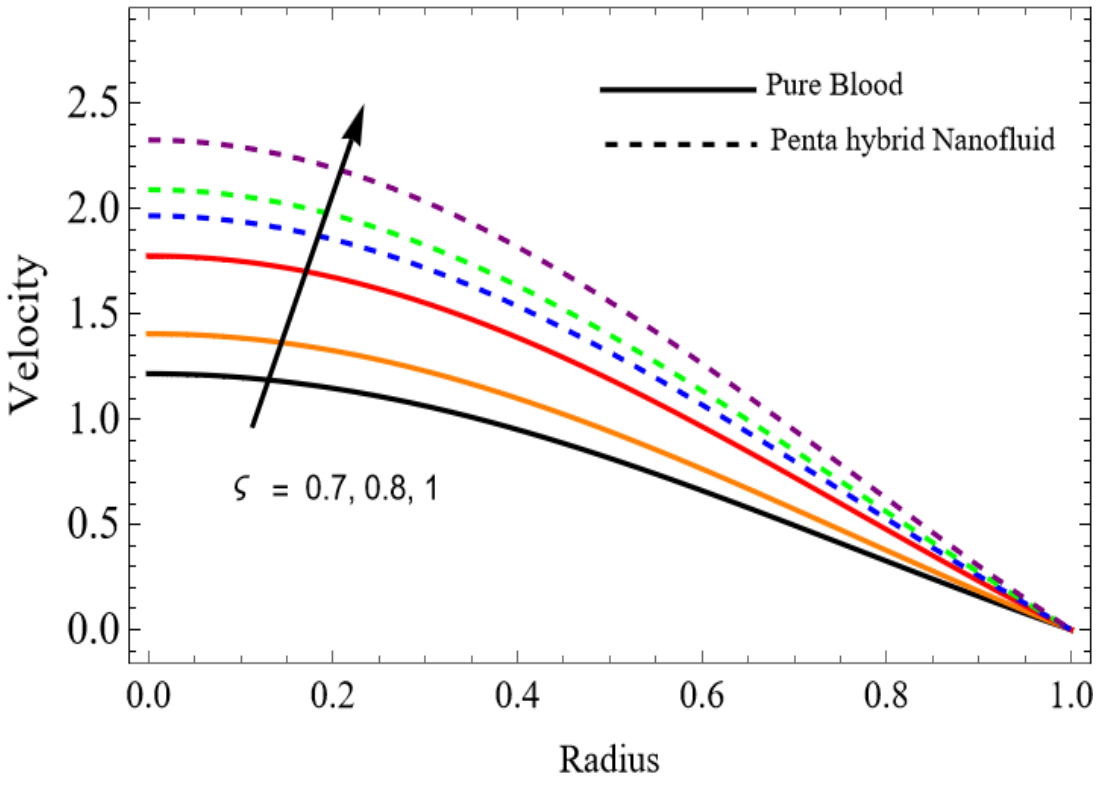


Figure 2. Velocity for ς.

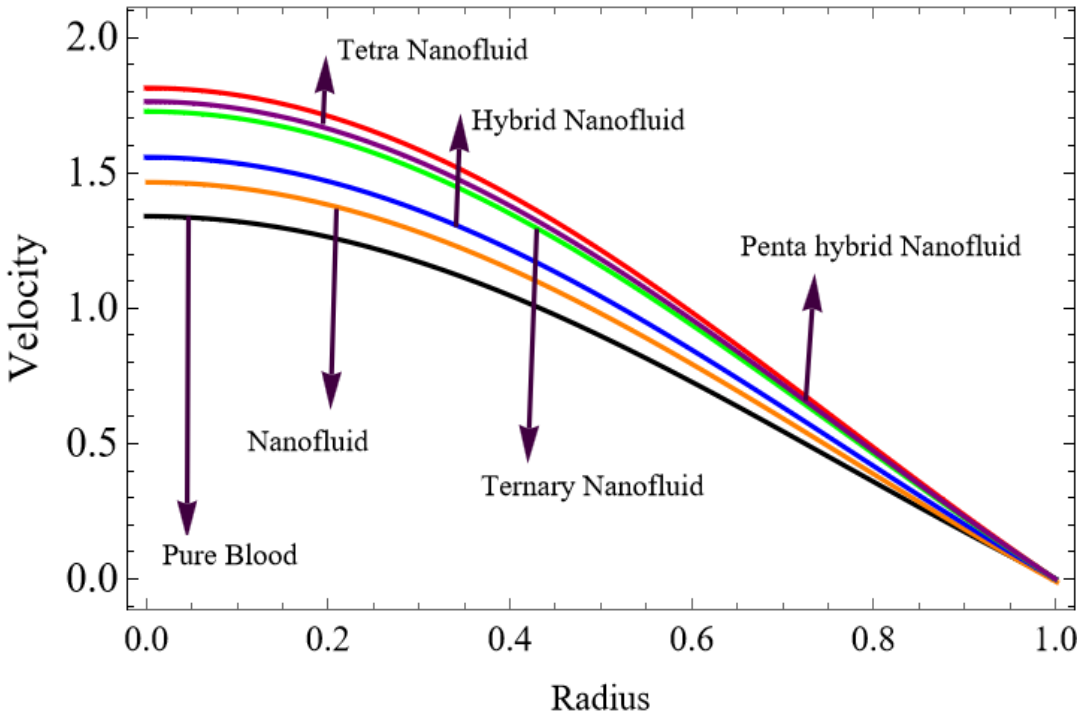


Figure 3. Velocity for Penta hybrid nanofluid.

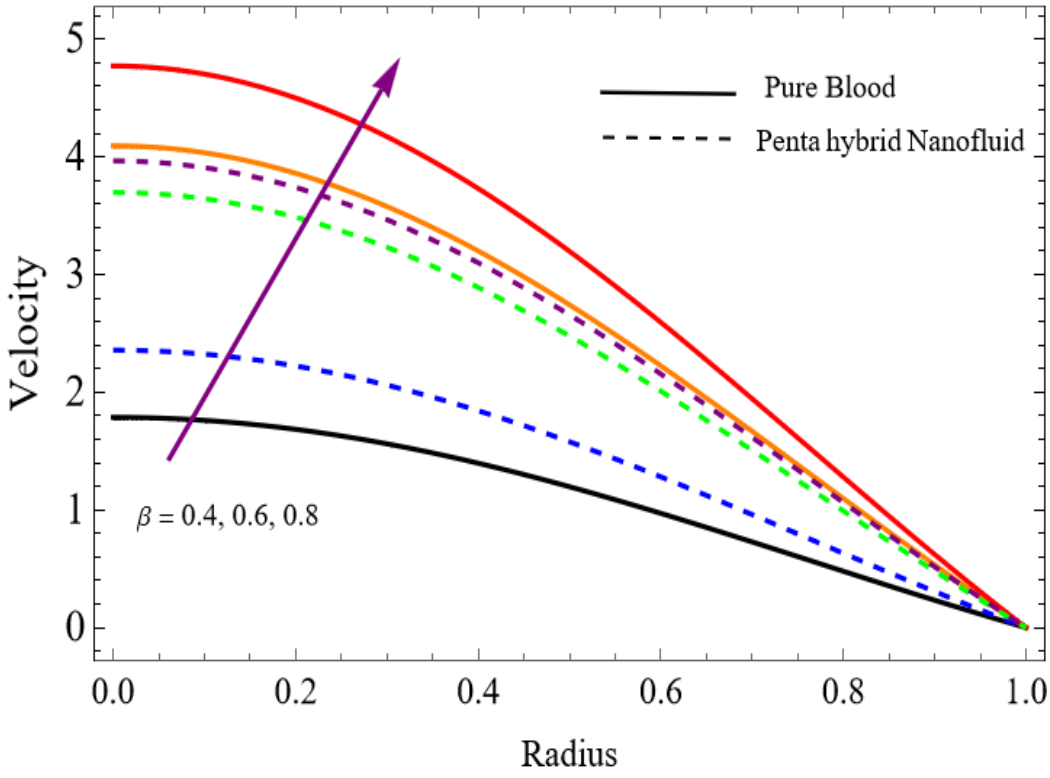


Figure 4. Velocity for β.

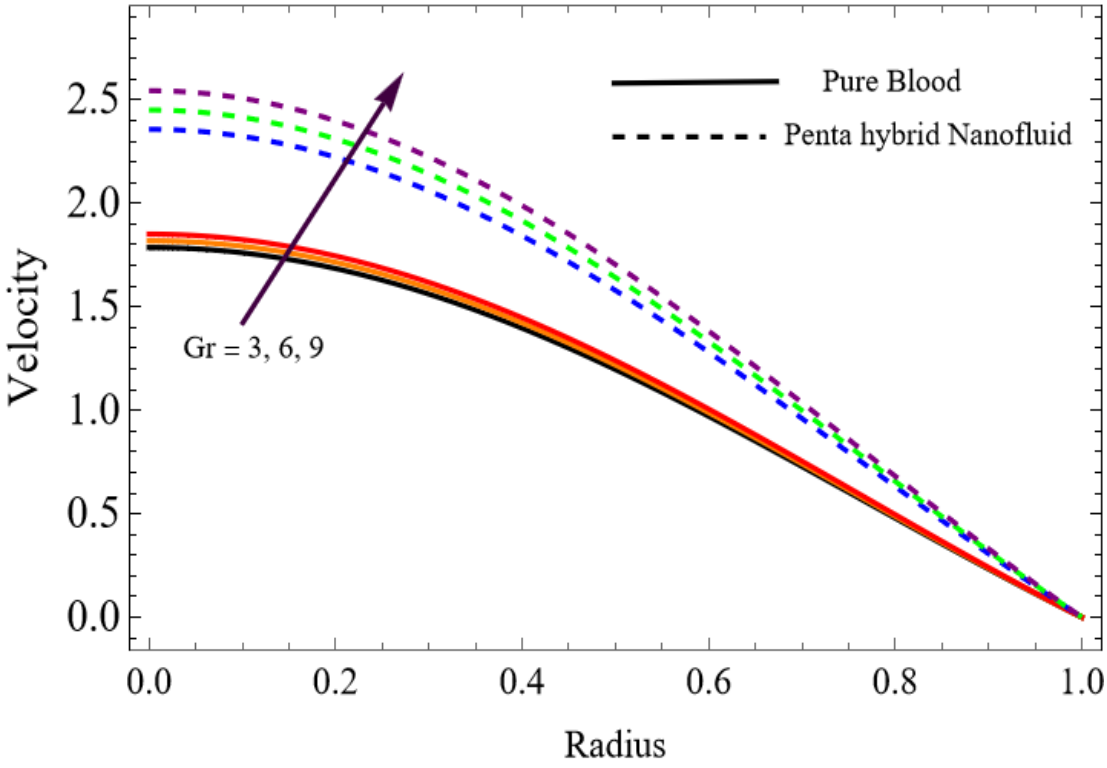


Figure 5. Velocity for *Gr*.

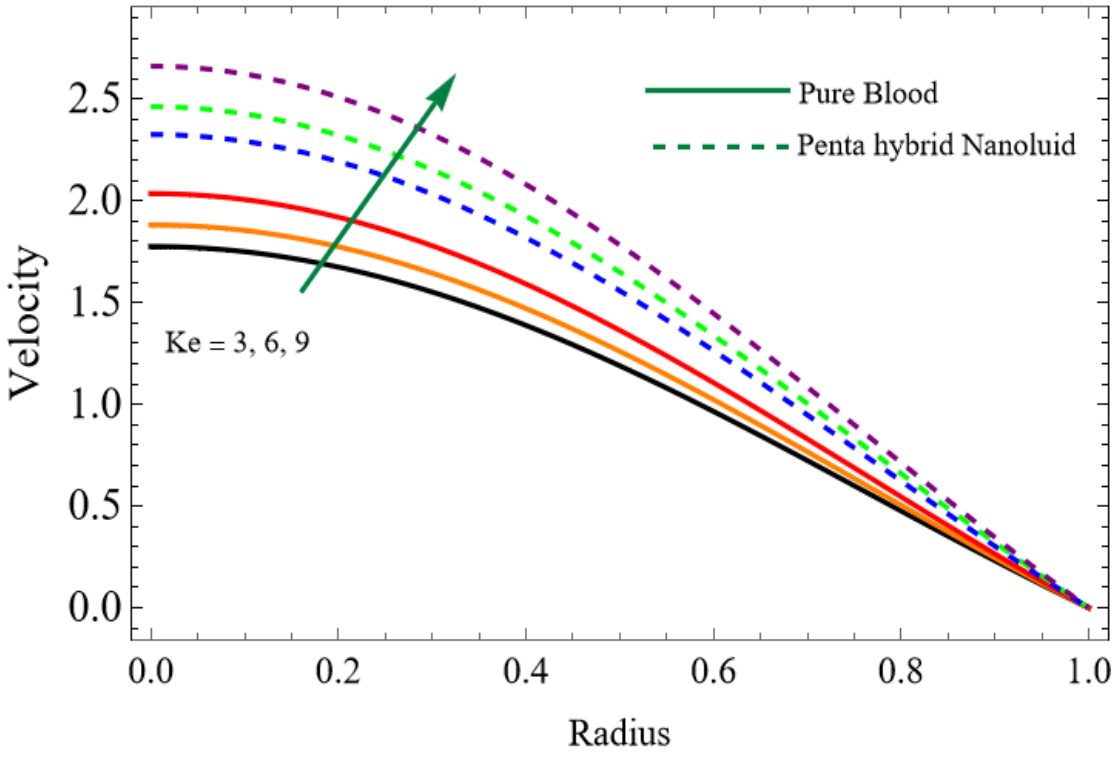


Figure 6. Velocity for *Ke*.

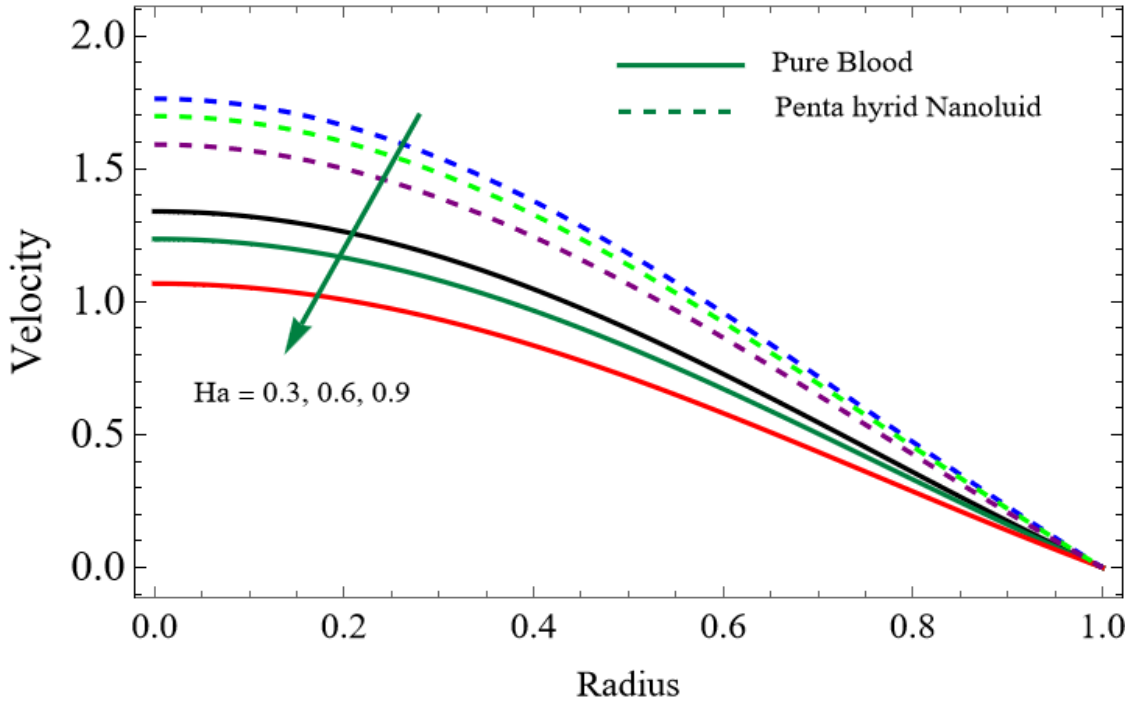


Figure 7. Velocity for *Ha*.

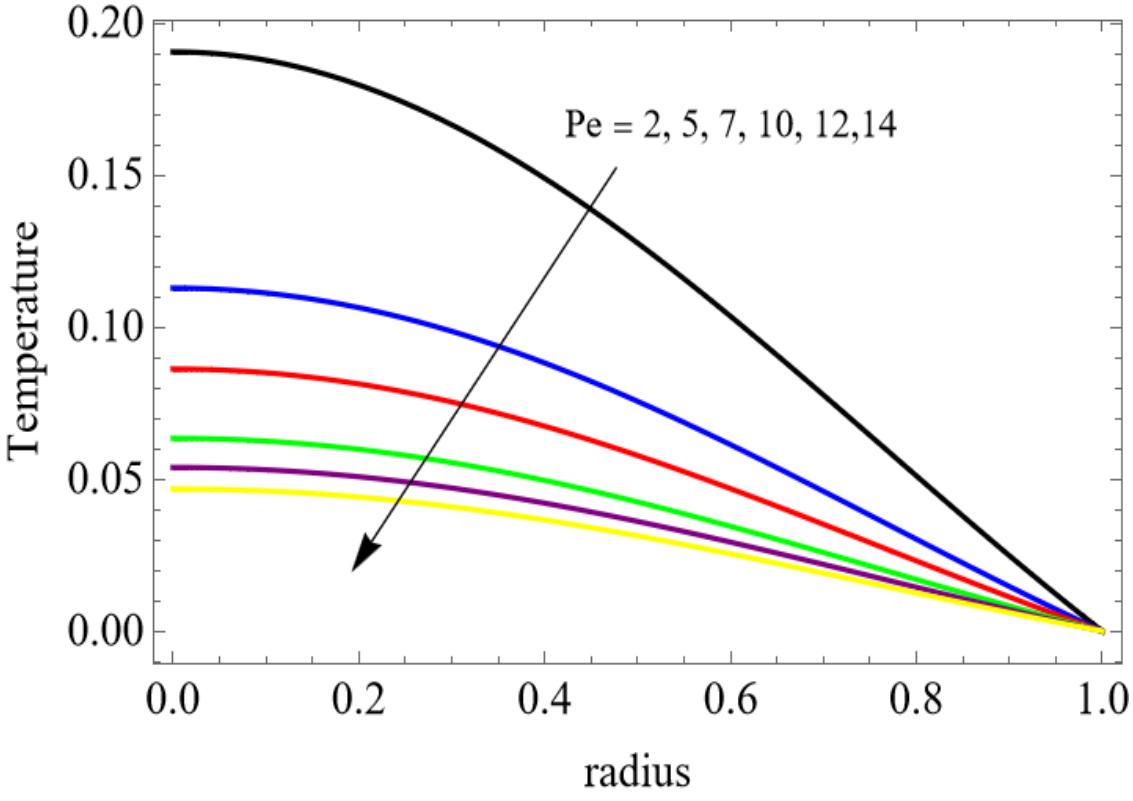


Figure 8. Temperature for *Pe*.

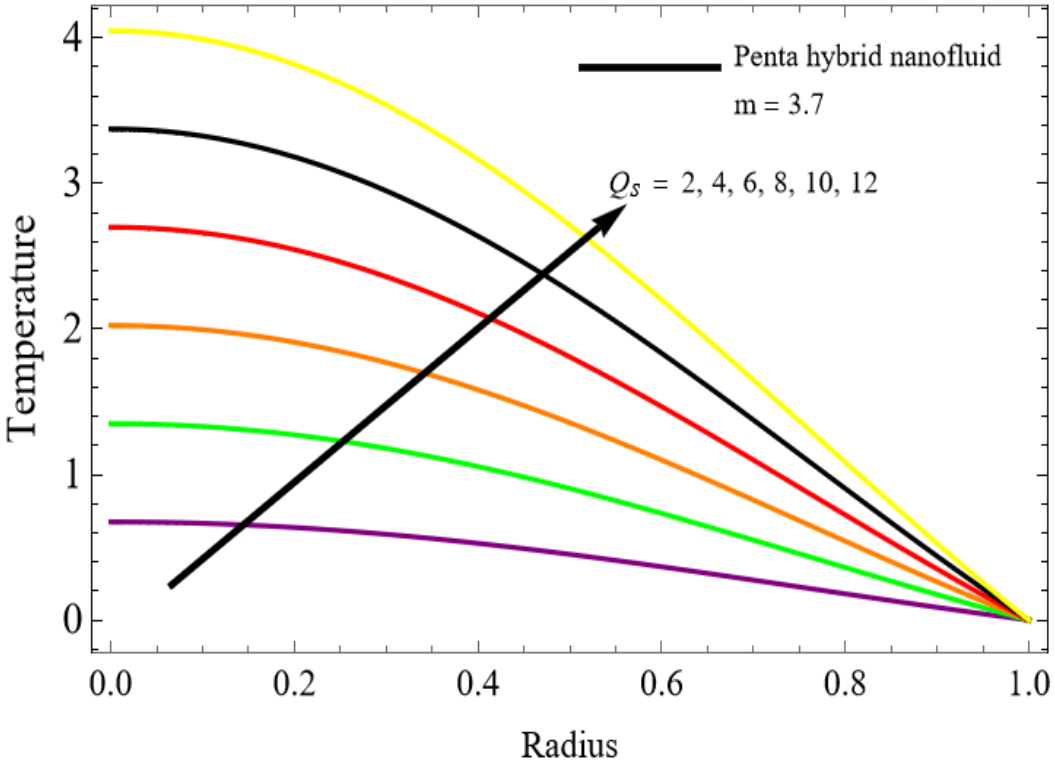


Figure 9. Temperature for Q_s.

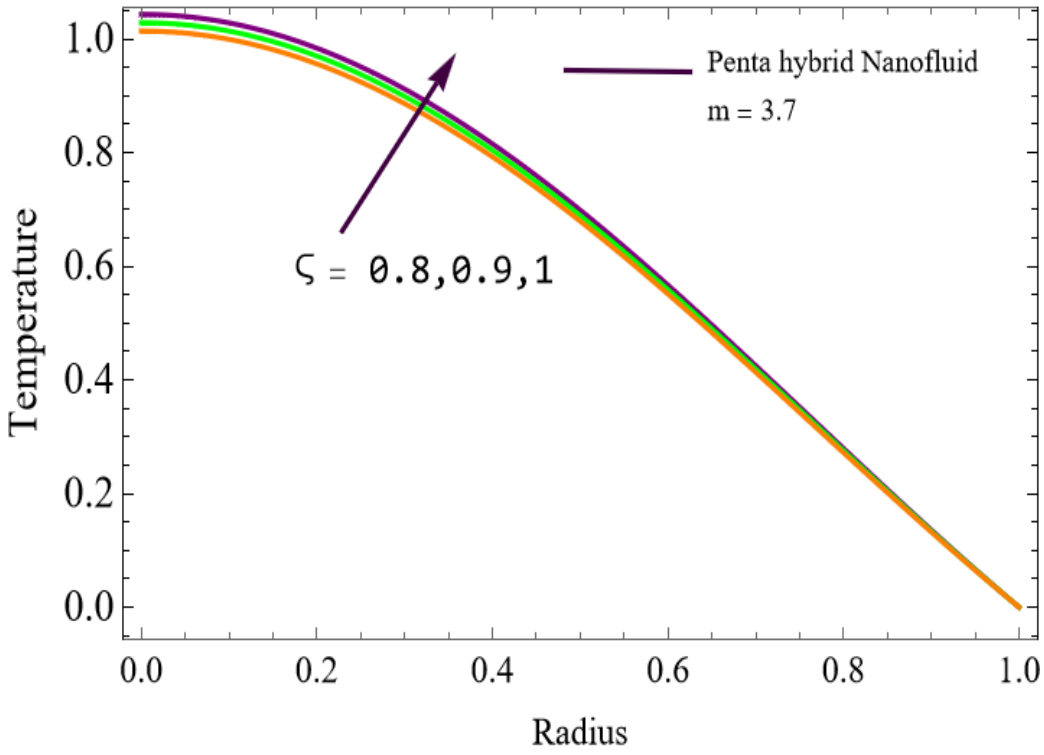
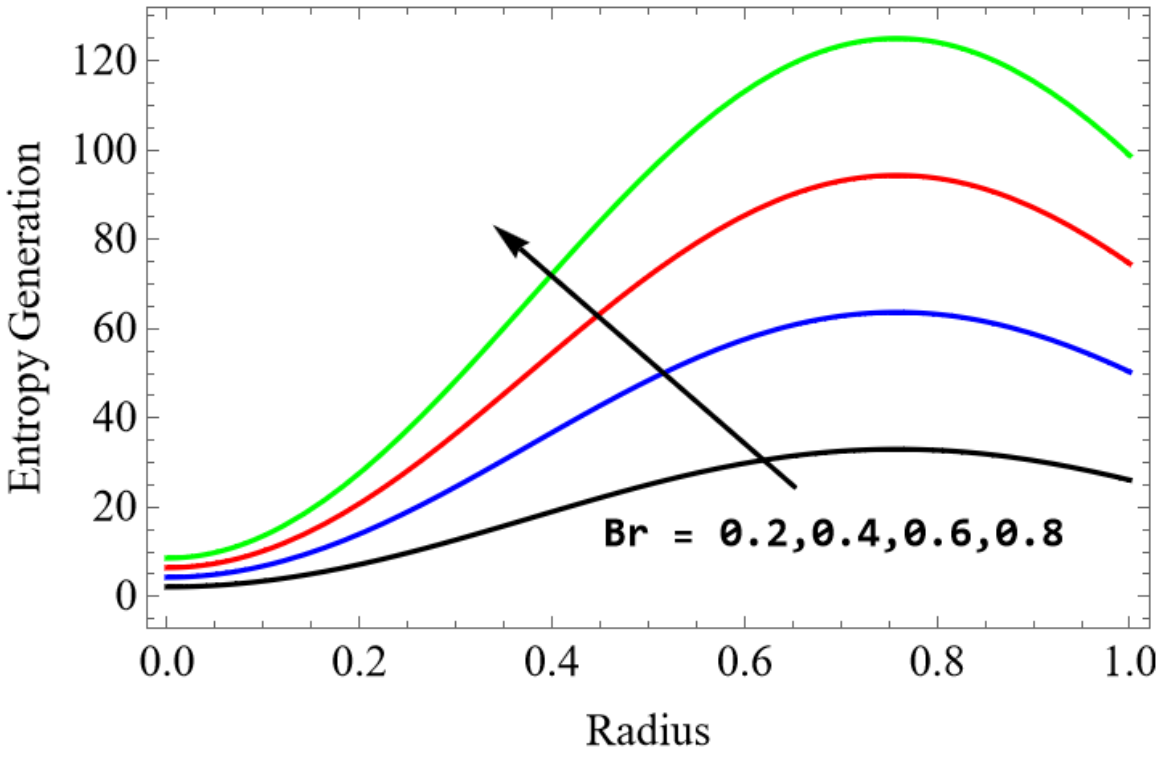
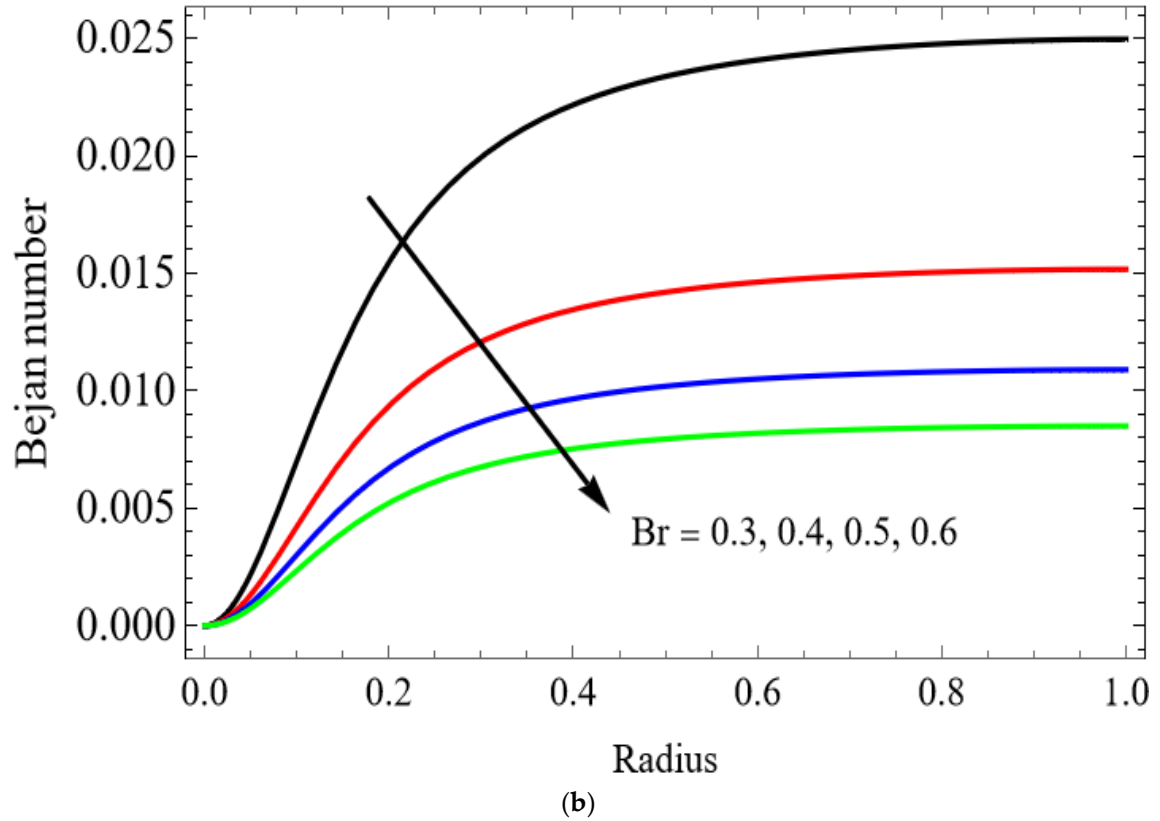


Figure 10. Temperature for ς.



(**a**)



(**b**)

Figure 11. (**a**) Entropy generation for *Br*. (**b**) Bejan number for *Br*.

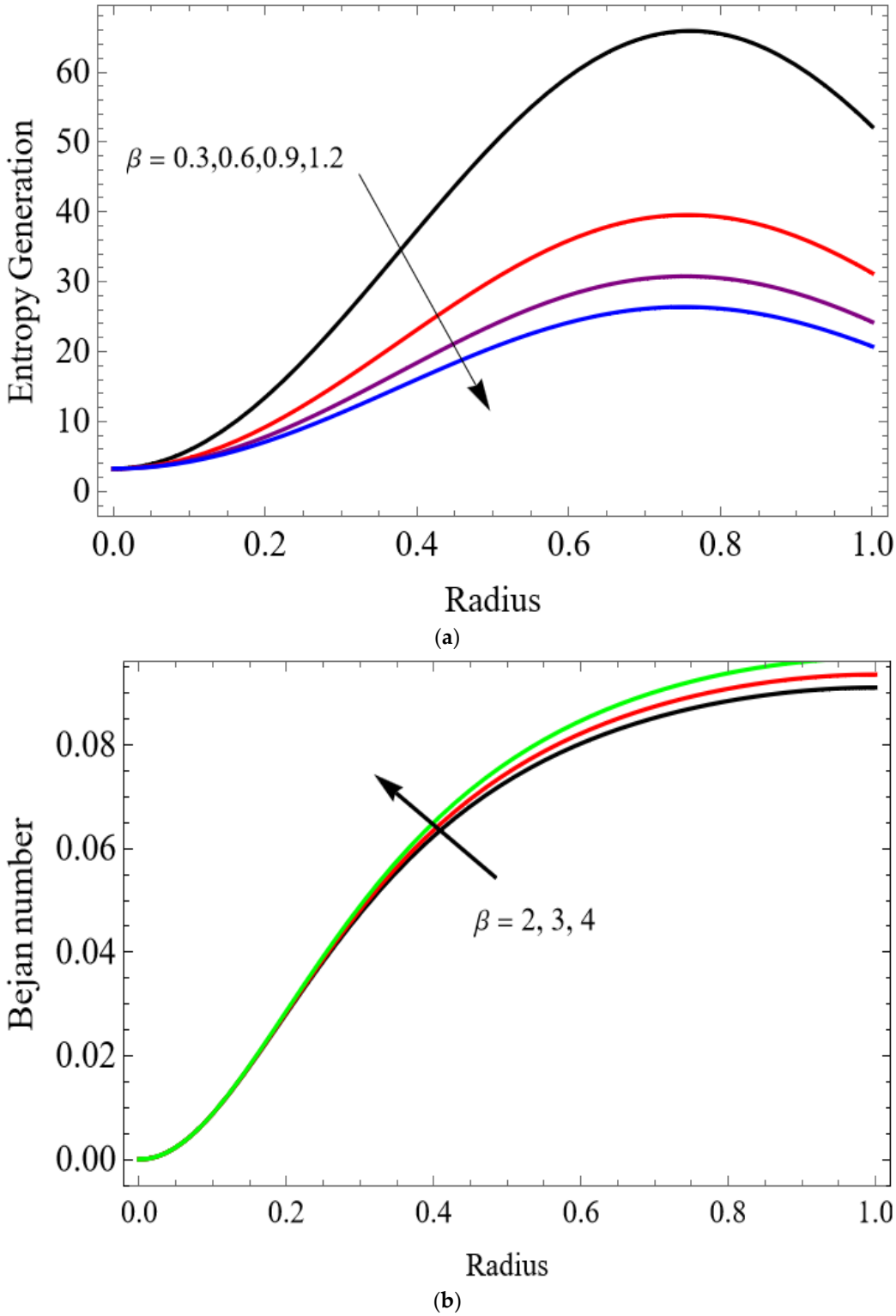


Figure 12. (**a**) Entropy generation for β. (**b**) Bejan number for β.

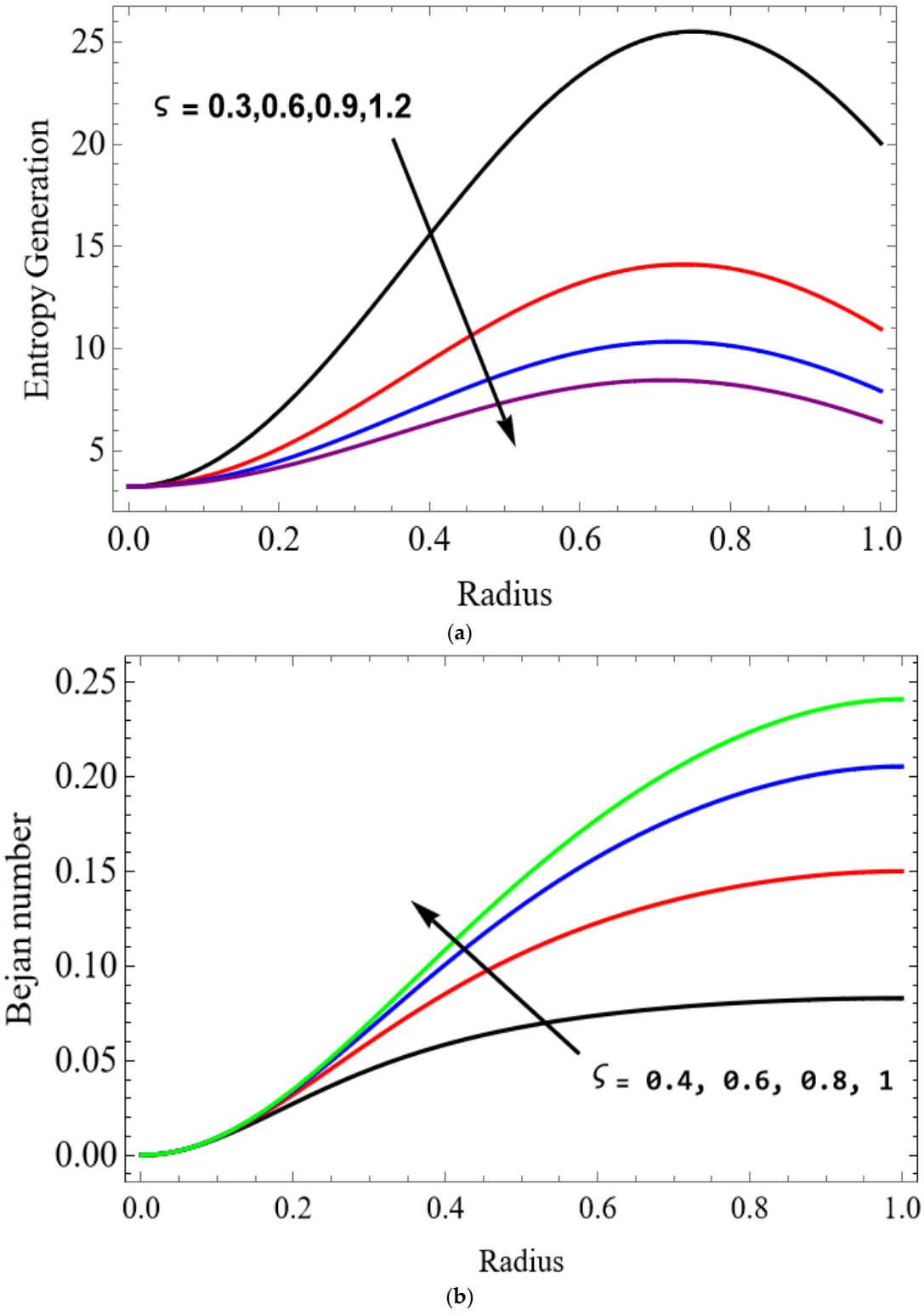


Figure 13. (**a**) Entropy generation for ς. (**b**) Bejan number for ς.

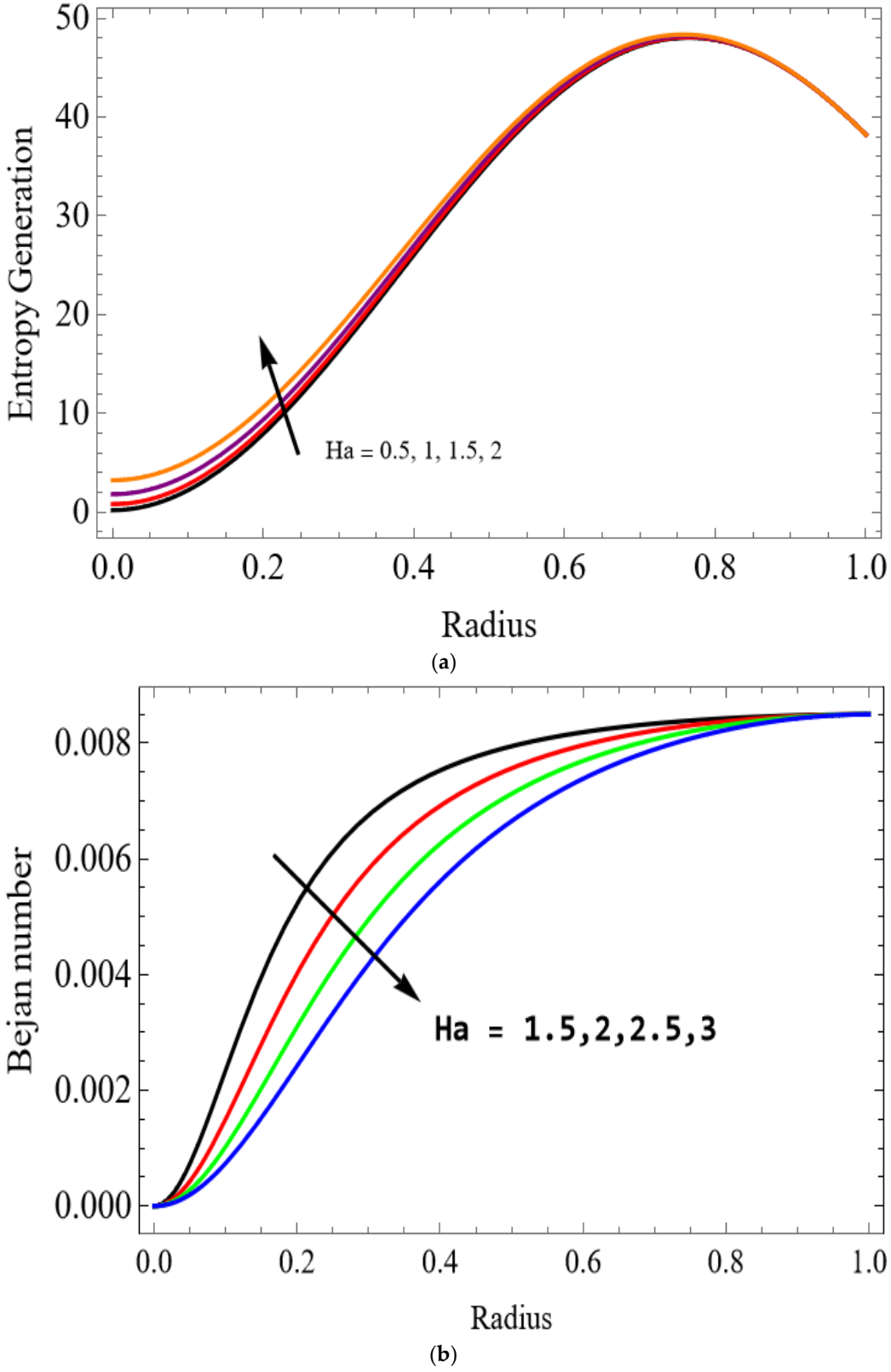


Figure 14. (**a**) Entropy generation for *Ha*. (**b**) Bejan number for *Ha*.

6. Conclusions

This research provides precise analytical solutions for fractional-order partial differential equations that describe the MHD unsteady Casson fluid flow in an inclined artery. To reflect the memory effects and to present a more realistic blood flow, especially under an external magnetic field, the Caputo–Fabrizio fractional derivative is used in the math-

ematical model. The closed-form solutions for the governing equations are arrived at by utilizing Laplace and finite Hankel transforms.

In order to improve the thermal behavior of the heat transfer medium, a novel class of nanofluids is used: penta-nanofluids, which contain five different types of nanoparticles. These nanoparticles remarkably enhance heat transport in comparison to pure fluids, single-nanoparticle (unitary) nanofluids, and even hybrid nanofluids.

Computer graphics generated by Mathematica software demonstrate the effects of several variables on the flow and temperature fields. The results show that thermal damping heavily influences both the fluid temperature and velocity. While velocity is increased when switching from simple nanofluids to penta-nanofluids, temperature shows the opposite behavior.

Specifically, integration of Caputo–Fabrizio fractional dynamics with penta-hybrid nanofluids in the present study has been shown to greatly facilitate heat transport and at the same time mitigate the increase in entropy generation (losses) in a stenosed arterial flow. Entropy-distributed bio-thermal systems, from the perspective of the present research, provide the basis for theoretical support of experimental and biomedical applications. It should be noted, however, that the present results are derived using simplifying assumptions, including laminar flow, constant uniform nanoparticle dispersion, a small degree of stenosis, and neglect of biochemical reactions and wall elasticity. Consequently, the results are only valid within the given framework of assumptions.

Funding: This research work was funded by Umm Al-Qura University, Saudi Arabia under grant number: 26UQU4331007GSSR01.

Informed Consent Statement: Not applicable.

Data Availability Statement: The original contributions presented in this study are included in the article. Further inquiries can be directed to the corresponding author.

Acknowledgments: The authors extend their appreciation to Umm Al-Qura University, Saudi Arabia for funding this research work through grant number: 26UQU4331007GSSR01.

Conflicts of Interest: The author declares no conflicts of interest.

Nomenclature

Symbol	Parameter Name	Physical Meaning/Significance
Re	Reynolds number	Ratio of inertial to viscous forces; characterizes laminar arterial flow
Bn	Casson parameter	Represents yield stress effects of blood rheology
M (Ha^2)	Magnetic parameter	Measures magnetic field induced Lorentz force
Gr	Grashof number	Ratio of buoyancy to viscous forces due to thermal gradients
Pr	Prandtl number	Ratio of momentum diffusivity to thermal diffusivity
Br	Brinkman number	Quantifies viscous dissipation effects
Ec	Eckert number	Conversion of kinetic energy into internal energy
Rd	Radiation parameter	Represents thermal radiation contribution
Qs	Heat source/sink parameter	Internal heat generation or absorption
Λ	Electro-osmotic parameter	Strength of electro-osmotic forcing
A	Fractional order parameter	Memory effect in Caputo–Fabrizio model
Φ_1–Φ_5	Nanoparticle volume fractions	Concentration of each nanoparticle in penta-hybrid nanofluid
Ns	Entropy generation number	Measure of irreversible energy losses
Be	Bejan number	Ratio of heat transfer irreversibility to total entropy generation

References

1. Choi, S.U.S. Enhancing thermal conductivity of fluids with nanoparticles. *ASME* **1995**, *66*, 99–105.
2. Ahmed, N.; Adnan Mohyud-Din, S.T.; Khan, U.; Nisar, K.S.; Baleanu, D.; Khan, I.; Nisar, K.S. A novel hybrid model for Cu–Al_2O_3/H_2O nanofluid flow and heat transfer in convergent/divergent channels. *Energies* **2020**, *13*, 1686. [CrossRef]

3. Mohyud-Din, S.T.; Ahmed, N.; Khan, U.; Khan, I.; Abdeljawad, T.; Nisar, K.S. Thermal transport investigation in magneto-radiative GO-MoS_2/H_2O-$C_2H_6O_2$ hybrid nanofluid subject to cattaneo–christov model. *Molecules* **2020**, *25*, 2592. [CrossRef]
4. Abbasi, A.; Al-Khaled, K.; Khan, M.I.; Khan, S.U.; El-Refaey, A.M.; Farooq, W.; Jameel, M.; Qayyum, S. Optimized analysis and enhanced thermal efficiency of modified hybrid nanofluid (Al_2O_3, CuO, Cu) with nonlinear thermal radiation and shape features. *Case Stud. Therm. Eng.* **2021**, *28*, 101425. [CrossRef]
5. Zhang, L.; Nazar, T.; Bhatti, M.M.; Michaelides, E.E. Stability analysis on the kerosene nanofluid flow with hybrid zinc/aluminum-oxide (ZnO-Al_2O_3) nanoparticles under Lorentz force. *Int. J. Numer. Methods Heat Fluid Flow* **2022**, *32*, 740–760. [CrossRef]
6. Nazar, T.; Bhatti, M.M.; Michaelides, E.E. Hybrid (Au-TiO_2) nanofluid flow over a thin needle with magnetic field and thermal radiation: Dual solutions and stability analysis. *Microfluid. Nanofluidics* **2022**, *26*, 2. [CrossRef]
7. Hafeez, M.B.; Krawczuk, M.; Nisar, K.S.; Jamshed, W.; Pasha, A.A. A finite element analysis of thermal energy inclination based on ternary hybrid nanoparticles influenced by induced magnetic field. *Int. Commun. Heat Mass Transf.* **2022**, *135*, 106074. [CrossRef]
8. Alharbi, K.A.M.; Ahmed, A.E.S.; Ould Sidi, M.; Ahammad, N.A.; Mohamed, A.; El-Shorbagy, M.A.; Bilal, M.; Marzouki, R. Computational valuation of darcy ternary-hybrid nanofluid flow across an extending cylinder with induction effects. *Micromachines* **2022**, *13*, 588. [CrossRef]
9. Elnaqeeb, T.; Animasaun, I.L.; Shah, N.A. Ternary-hybrid nanofluids: Significance of suction and dual-stretching on three-dimensional flow of water conveying nanoparticles with various shapes and densities. *Z. Naturforsch. A* **2021**, *76*, 231–243. [CrossRef]
10. Tzirtzilakis, E.E. A mathematical model for blood flow in magnetic field. *Phys. Fluids* **2005**, *17*, 077103. [CrossRef]
11. Chato, J.C. Heat transfer to blood vessels. *J. Biomech. Eng.* **1980**, *102*, 110–118. [CrossRef]
12. Shaw, S.; Murthy, P.V.S.N. Magnetic drug targeting in the permeable blood vessel—The effect of blood rheology. *J. Nanotechnol. Eng. Med.* **2010**, *1*, 021001. [CrossRef]
13. Shahzad, M.H.; Ahammad, N.A.; Nadeem, S.; Awan, A.U.; Guedri, K.; Alamer, A.; Fadhl, B.M. Non-Newtonian blood flow across stenosed elliptical artery: Case study of nanoparticles for brain disabilities with fuzzy logic. *Mod. Phys. Lett. B* **2025**, *39*, 2450470. [CrossRef]
14. Abbas, Z.; Goher, S.; Shabbir, M.S. Analysis of biological mechanism of blood flow containing nanoparticles through an arterial stenosis. *Waves Random Complex Media* **2023**, *23*, 1–20. [CrossRef]
15. Shit, G.C.; Majee, S. Pulsatile flow of blood and heat transfer with variable viscosity under magnetic and vibration environment. *J. Magn. Magn. Mater.* **2015**, *388*, 106–115. [CrossRef]
16. Akbar, N.S.; Butt, A.W. Entropy generation analysis in convective ferromagnetic nano blood flow through a composite stenosed arteries with permeable wall. *Commun. Theor. Phys.* **2017**, *67*, 554. [CrossRef]
17. MacDonald, D.A. On steady flow through modelled vascular stenoses. *J. Biomech.* **1979**, *12*, 13–20. [CrossRef]
18. Caro, C.G.; Pedley, T.J.; Schroter, R.C.; Seed, W.A.; Parker, K.H. The systemic arteries. In *The Mechanics of the Circulation*; Cambridge University Press: Cambridge, UK, 2012; pp. 238–342.
19. Liepsch, D.W. Flow in tubes and arteries-a comparison. *Biorheology* **1986**, *23*, 395–433. [CrossRef]
20. Srivastava, L.M.; Srivastava, V.P. Peristaltic transport of blood: Casson model—II. *J. Biomech.* **1984**, *17*, 821–829. [CrossRef]
21. Nagarani, P.; Sarojamma, G.; Jayaraman, G. Exact analysis of unsteady convective diffusion in Casson fluid flow in an annulus–Application to catheterized artery. *Acta Mech.* **2006**, *187*, 189–202. [CrossRef]
22. Venkatesan, J.; Sankar, D.S.; Hemalatha, K.; Yatim, Y. Mathematical analysis of Casson fluid model for blood rheology in stenosed narrow arteries. *J. Appl. Math.* **2013**, *2013*, 583809. [CrossRef]
23. Hayat, T.; Asad, S.; Alsaedi, A. Flow of Casson fluid with nanoparticles. *Appl. Math. Mech.* **2016**, *37*, 459–470. [CrossRef]
24. Ali, F.; Sheikh, N.A.; Khan, I.; Saqib, M. Magnetic field effect on blood flow of Casson fluid in axisymmetric cylindrical tube: A fractional model. *J. Magn. Magn. Mater.* **2017**, *423*, 327–336. [CrossRef]
25. He, S.; Fataf, N.A.A.; Banerjee, S.; Sun, K. Complexity in the muscular blood vessel model with variable fractional derivative and external disturbances. *Phys. A Stat. Mech. Its Appl.* **2019**, *526*, 120904. [CrossRef]
26. Vardanyan, V.A. Effect of magnetic field on blood flow. *Biofizika* **1973**, *18*, 491–496.
27. Akbar, N.S.; Butt, A.W. Magnetic field effects for copper suspended nanofluid venture through a composite stenosed arteries with permeable wall. *J. Magn. Magn. Mater.* **2015**, *381*, 285–291. [CrossRef]
28. Mekheimer, K.S.; Mohamed, M.S.; Elnaqeeb, T. Metallic nanoparticles influence on blood flow through a stenotic artery. *Int. J. Pure Appl. Math.* **2016**, *107*, 201–220. [CrossRef]
29. Wong, P.K.; Wang, T.-H.; Deval, J.H.; Ho, C.-M. Electrokinetics in micro devices for biotechnology applications. *IEEE/ASME Trans. Mechatron.* **2004**, *9*, 366–376. [CrossRef]
30. Burgreen, D.; Nakache, F.R. Electrokinetic flow in ultrafine capillary slits[1]. *J. Phys. Chem.* **1964**, *68*, 1084–1091. [CrossRef]
31. Saravani, M.S.; Kalteh, M. Heat transfer investigation of combined electroosmotic/pressure driven nanofluid flow in a microchannel: Effect of heterogeneous surface potential slip boundary condition. *Eur. J. Mech.-B/Fluids* **2020**, *80*, 13–25. [CrossRef]

32. Rashidi, M.M.; Bhatti, M.M.; Abbas, M.A.; Ali, M.E.S. Entropy generation on MHD blood flow of nanofluid due to peristaltic waves. *Entropy* **2016**, *18*, 117. [CrossRef]
33. Farooq, S.; Hayat, T.; Khan, M.I.; Alsaedi, A. Entropy generation minimization (EGM) in magneto peristalsis with variable properties. *Comput. Methods Programs Biomed.* **2020**, *186*, 105045. [CrossRef] [PubMed]
34. Zhang, L.; Bhatti, M.M.; Marin, M.; Mekheimer, K.S. Entropy analysis on the blood flow through anisotropically tapered arteries filled with magnetic zinc-oxide (ZnO) nanoparticles. *Entropy* **2020**, *22*, 1070. [CrossRef]
35. Karmakar, P.; Ali, A.; Das, S. Circulation of blood loaded with trihybrid nanoparticles via electro-osmotic pumping in an eccentric endoscopic arterial canal. *Int. Commun. Heat Mass Transf.* **2023**, *141*, 10659. [CrossRef]
36. Abdulhameed, M.; Babagana, B.; Markus, S.; Yakubu, D.G.; Adamu, G.T. The Effects of Fractional Relaxation Time and Magnetic Field on Blood Flow through Arteries along with Nanoparticles. *Defect Diffus. Forum* **2023**, *424*, 59–76. [CrossRef]

Disclaimer/Publisher's Note: The statements, opinions and data contained in all publications are solely those of the individual author(s) and contributor(s) and not of MDPI and/or the editor(s). MDPI and/or the editor(s) disclaim responsibility for any injury to people or property resulting from any ideas, methods, instructions or products referred to in the content.